Title

NEAR-THRESHOLD FATIGUE CRACK PROPAGATION IN ULTRA-HIGH STRENGTH STEEL: INFLUENCE OF LOAD RATIO AND CYCLIC STRENGTH

Author

Ritchie, Robert O.

Publication Date

1976-10-01

Submitted to Journal of Engineering Materials and Technology, Transactions of the American Society of Mechanical Engineers, Series H

LBL-5496
Preprint

NEAR-THRESHOLD FATIGUE CRACK PROPAGATION IN ULTRA-HIGH STRENGTH STEEL: INFLUENCE OF LOAD RATIO AND CYCLIC STRENGTH

Robert O. Ritchie

October 1976

Prepared for the U. S. Energy Research and Development Administration under Contract W-7405-ENG-48

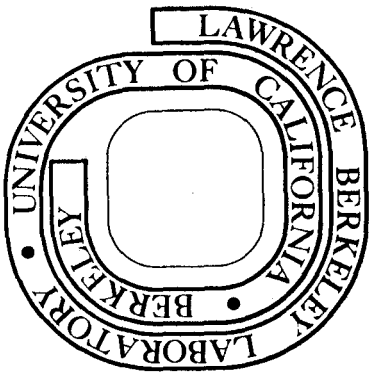

DISCLAIMER

Submitted to Journal of Engineering Materials and Technology, Trans. ASME, Series H.

LBL-5496
October, 1976

NEAR-THRESHOLD FATIGUE CRACK PROPAGATION IN ULTRA-HIGH STRENGTH STEEL: INFLUENCE OF LOAD RATIO AND CYCLIC STRENGTH

Robert O. Ritchie*
Assistant Professor
Department of Mechanical Engineering
Massachusetts Institute of Technology
Cambridge, Massachusetts 02139

*Formally of the Department of Materials Science and Engineering, University of California in Berkeley, Ca., 94720.

NEAR-THRESHOLD FATIGUE CRACK PROPAGATION IN ULTRA-HIGH STRENGTH STEEL: INFLUENCE OF LOAD RATIO AND CYCLIC STRENGTH

Robert O. Ritchie*

Materials and Molecular Research Division, Lawrence Berkeley Laboratory
and Department of Materials Science and Engineering,
University of California, Berkeley, California 94720

ABSTRACT

Fatigue crack propagation behavior of an ultra-high strength steel (300-M) has been investigated in humid air over a very wide spectrum of growth rates from 10^{-8} to 10^{-1} mm/cycle. Particular emphasis has been devoted to the influence of mean stress (or load ratio $R = K_{min}/K_{max}$) and microstructure on fatigue crack growth near the threshold stress intensity for crack propagation, ΔK_o. Increasing the load ratio from R = 0.05 to 0.70 was found to lead to increased near-threshold growth rates, and a decrease in the threshold stress intensity. Similarly, increasing material strength, by varying the microstructure through quench and tempering and isothermal transformation, resulted in higher near-threshold growth rates, and a marked reduction in ΔK_o. These effects are contrasted with behavior at higher growth rates. The influence of strength on ΔK_o is rationalized in terms of the cyclic hardening or softening response of the material, and hence it is shown that cyclic softening can be beneficial to fatigue crack propagation resistance at very low growth rates.

A model is developed to account for the effect of strength and load ratio on the threshold stress intensity, ΔK_o, in steels, based on a critical fracture stress criterion for crack growth modified by the influence of hydrogen, and the results discussed in the light of crack closure and environmental theories for near-threshold fatigue crack propagation in moist air.

---

*Now at Department of Mechanical Engineering, Massachusetts Institute of Technology, Cambridge, Massachusetts 02139.

INTRODUCTION

Since fracture mechanics was first applied to the problem of fatigue crack growth in metals in the early 1960's [1],[1] an immense amount of information has been accumulated relating rates of fatigue crack propagation to such variables as mean stress, microstructure, environment, stress state, etc. [eg. 1-12]. Concurrent with this research, a general framework for understanding the fracture mechanisms has emerged, permitting attempts to be made to relate these mechanisms to macroscopic crack growth behavior. One area, however, which has received comparatively little attention is the slow growth of fatigue cracks at rates less than 10^{-5} to 10^{-6} mm/cycle. This is unfortunate since the major portion of the lifetime of a cracked component is often spent in this region. Not only is there little understanding of the growth mechanisms at very low crack propagation rates, but there is a substantial lack of reliable engineering data. Such information, particularly a knowledge of a threshold stress intensity below which cracks cannot propagate, would be essential in the design of components subject to extreme high frequency, low amplitude loadings for lifetimes of 10^{10} to 10^{12} cycles [2].

Most studies have confirmed that fatigue crack growth is primarily controlled by the alternating stress intensity, ΔK, through an expression [1] of the form:

$$\frac{da}{dN} = C\,\Delta K^{m} \quad , \tag{1}$$

[1] Numbers in brackets designate References at end of paper.

where 'C' and 'm' are assumed to be constants, da/dN is the fatigue crack growth rate per cycle, and ΔK is given by the difference between the maximum and minimum stress intensities for each cycle, i.e., $\Delta K = K_{max} - K_{min}$. This expression adequately describes behavior for the mid-range of growth rates, typically 10^{-5} to 10^{-3} mm/cycle, but often underestimates the propagation rate at higher growth rates, as K_{max} approaches K_{Ic}, the fracture toughness. Similarly, the expression is found to be conservative at lower growth rates where ΔK approaches a threshold stress intensity ΔK_o, below which crack propagation cannot be detected [7-12].

This sigmoidal variation of growth rate with ΔK can, however, be rationalized in terms of the primary crack growth mechanisms involved (Fig. 1). In steels, for the mid-range of growth rates, (regime B), failure generally occurs by a transgranular ductile striation mechanism [3], and the rate of crack growth is thought to be largely insensitive to microstructure and mean stress (characterized by the load ratio, $R = K_{min}/K_{max}$) [4-6]. Large effects of microstructure and load ratio, however, predominate in the high and low growth rate regimes (regimes C and A respectively). At high growth rates the effect is ascribed to the occurrence of superimposed static modes of fracture, such as cleavage, intergranular and micro-void coalescence, accompanying or replacing striation growth [4-6]. At very low (near-threshold) growth rates, the explanation of the microstructure and load ratio effect remains uncertain, although it is clear that the nature of the test environment can play a major role [7, 8]. Mechanisms of growth in this region have been observed to be microstructurally sensitive,

involving the occurrence of environmentally induced fracture modes such as intergranular fracture in steels [6,7] and cleavage fracture in titanium alloys [8]. However, it has not as yet been established which microstructures are beneficial in improving resistance to low growth rate fatigue failure.

The aim of the present research is to characterize microstructural influences on near-threshold fatigue crack growth in an attempt to provide some basis for the design of alloys more resistant to very high cycle fatigue failure. For the lack of any previous guidelines, this paper describes initial experiments to assess the influence of materials strength on near-threshold fatigue crack growth at different load ratios, and to determine how cyclic hardening or softening might modify this effect.

EXPERIMENTAL

The steel investigated was an ultra-high strength, aircraft-quality (vacuum-arc remelted), 300-M, received in the fully-annealed condition, and having the following composition (wt.%)

C	Mn	Cr	Ni	Mo	Si	S	P	V
0.42	0.76	0.76	1.76	0.41	1.59	0.002	0.007	0.10

The composition is essentially that of AISI 4340 modified with 1.4% silicon.

The material was austenitized at 870°C for 1 hr and quenched into agitated oil, to yield a prior austenite grain size of 20 μm. Specimens were subsequently tempered for 1 hr at temperatures of 100, 300, 470 and 650°C to provide a wide variation in strength. These treatments are hereafter referred to as T100, T300, T470, and T650, respectively. Two further heat treatments were employed, namely, i) austenitizing at 870°C, isothermally holding for 1 hr at 250°C (20°C below M_s), and tempering at 300°C (referred to as ISO250), and ii) tempering at 300°C after oil quenching from 1200°C (referred to as A1200). Full details of fatigue crack growth in the latter structure are given elsewhere [12].

Fatigue testing was performed using 12.7 mm thick 1-T C.T.S. specimens, cycled under load control on 100 kN electro servo-hydraulic M.T.S. testing machines, under sinusoidal tension at load ratios ($R = K_{min}/K_{max}$) of 0.05 and 0.70. The environment for all tests was laboratory air, maintained at constant temperature (23°C) and constant relative humidity (45%). Crack lengths were continuously monitored using the electrical

potential technique [13], capable of measuring crack length to within 0.1 mm, and to detect changes in crack length of the order of 0.01 mm. Growth rates were computed by numerical differentiation of crack length versus number of cycles data, curve-fitted using finite difference and incremental-step polynomial procedures [5].

The threshold, ΔK_o, was calculated in terms of the stress intensity at which no growth occurred within 10^7 cycles. Since the crack monitoring technique is at least accurate to 0.1 mm, this corresponds to a maximum growth rate of 10^{-8} mm/cycle (4×10^{-10} in/cycle). Thresholds were approached using a successive load reduction (of not greater than 10% reduction in K_{max} at every step), followed by crack growth procedure to avoid residual stress effects. Measurements were taken, at each load level, over increments of crack growth of 1 - 1.5 mm, representing a distance of between 100 to 1000 times the maximum plastic zone size at the previous load. Following threshold ΔK_o measurements, the load was increased in steps and the same procedure followed. For comparison, tests were also conducted at intermediate and high growth rates to yield propagation rate data between 10^{-8} to 10^{-1} mm/cycle. All fatigue tests were performed at 50 Hz, except high growth rate tests (greater than 10^{-4} mm/cycle) which were run at 5 Hz. No frequency effects were observed at such high propagation rates. Plane strain conditions were maintained in all fatigue tests, except in the T650 condition for K_{max} greater than 80 MPa$\sqrt{m}$.

Monotonic tensile tests were performed on 25.4 mm gage uniaxial tensile bars, and plane strain fracture toughness (K_{Ic}) tests using

20-25 mm thick 1-T C.T.S. specimens, according to the appropriate A.S.T.M. standards. Cyclic stress-strain data were determined from 12.7 mm gage tensile bars, cycled under strain control at R = -1, using the incremental-step procedure [14]. All specimens were machined in the longitudinal (L-T) orientation.

Magnetic saturation induction measurements, using a permeameter [15], were made during monotonic tensile tests of sheet specimens to assess the extent of any deformation-induced austenite-to-martensite transformation. Microstructure and fracture morphology was characterized using transmission and scanning electron microscopy.

RESULTS

The variations of monotonic yield and tensile strength, and of plane strain fracture toughness (K_{Ic}) with tempering temperature for 300-M, quenched from 870°C, are shown in Figs. 2 and 3, respectively. Optimum strength and toughness was achieved after tempering at 300°C (T300), the commercially-used heat-treatment. The T100, T470, and ISO250 conditions were selected to show identical (monotonic) yield strength, with different strain hardening, ductility and toughness properties. Ambient temperature mechanical properties (monotonic) of the structures tested are listed in Table 1.

Before discussing the fatigue data it is necessary at this stage to briefly summarize the microstructures of the material tested. Quenched and tempered structures were typical of tempered lath martensite with some evidence of twinned plates. The T100 structure contained a high dislocation density, autotempered carbides and about 6% retained austenite,[1] present as thin films, roughly 200Å thick, surrounding martensite laths. Evidence of ε-carbide precipitation could also be seen in the T300 structure, the retained austenite level dropping to approximately 4%. The carbide was present as interlath cementite precipitates in the T470 structure, and less than 1% retained austenite could be detected. In the T650 structure, the cementite had spheroidized, and all retained austenite had transformed. The ISO250 structure, however, contained a much increased proportion of retained austenite,

[1] measured by magnetic saturation.

Table 1. Mechanical Properties (monotonic) of 300-M Steel.

Code	Austenitizing Treatment	Temper	0.2% Proof Stress (MPa)	U.T.S. (MPa)	Elongation[1] (percent)	True Fracture Strain	K_{Ic} (MPa$\sqrt{m}$)	Grain Size[2] (μm)
T100	870°C, oil quench	100°C	1497	2338	12.4	0.29	35.5	20
T300	870°C, oil quench	300°C	1737	2006	11.9	0.66	65.1	20
T470	870°C, oil quench	470°C	1497	1683	12.1	0.69	68.9	20
T650	870°C, oil quench	650°C	1074	1186	18.1	0.81	(185)[3]	20
A1200	1200°C, oil quench	300°C	1657	1986	6.3	0.22	80.3	160
ISO250	870°C, isothermally held at 250°C, oil quench.	300°C	1497	1862	14.5	-	88.5	20

1. Total elongation measured on a 25.4 mm (1-inch) gage length.

2. Prior austenite grain size, determined by linear intercept method.

3. Invalid K_{Ic} result, estimated using equivalent energy procedure [16].

of the order of 12%, distributed as a network of interlath films 300-400Å thick within a lower bainite/martensite structure.

Fatigue crack propagation data are presented in the form of growth rate curves of da/dN versus ΔK, plotted on logarithmic scales over a range of growth rates from 10^{-8} to 10^{-1} mm/cycle ($<10^{-9}$ to 10^{-3} in/cycle). Results for quenched and tempered steel are shown in Figs. 4 and 5, at R = 0.05 and 0.70 respectively, and for isothermally transformed steel (ISO250) in Fig. 6. It is apparent from these plots that the influence of load ratio (R) and of different microstructures on fatigue crack growth behavior is maximized at low and at high stress intensities (i.e., in regimes A and C of Fig. 1). Each regime is now considered in turn.

i) Intermediate Growth Rate Regime B

For the mid-range of growth rates represented by the linear portion of the growth rate curves where Eq. (1) is valid, little variation in propagation rate can be seen between different microstructures at both load ratios. Growth rates curves tend toward a common line of slope (i.e., exponent 'm' in Eq. 1) of 2.54 at R = 0.05 and 2.67 at R = 0.70. In this range the mechanism of fatigue failure in all structures was found to be primarily transgranular ductile striation growth (Fig. 7a), consistent with a lack of microstructural and load ratio sensitivity on growth rate behavior [5,6]. Considering the wide variation of tensile strength (2-fold) and toughness (6-fold) shown by the structures tested, fatigue crack growth in regime B appears independent of such mechanical properties.

ii) High Growth Rate Regime C

At higher stress intensities, growth rate curves display an acceleration in propagation rate, as K_{max} approaches K_{Ic}, which is characteristic of regime C. As clearly demonstrated in Fig. 6, marked effects of load ratio and microstructure are now observed. Faster crack propagation rates and a larger load ratio effect (at a given ΔK) are shown as the toughness of the structure is reduced. Fractography of failures in this region confirmed the presence of static modes, as shown in Fig. 7. Areas of fibrous fracture were present in all structures (eg. Fig. 7b and c), with additional intergranular cracking in the T470 condition, and intergranular and cleavage cracking in T100 (Fig. 7b).

It is clear that, in this region, the onset of growth, which is both sensitive to microstructure and load ratio, is dependent on the toughness, and arises from the occurrence of static fracture mechanisms during striation growth.

iii) Low Growth Regime A

The largest influence of load ratio and microstructure can be seen at low stress intensities in regime A, where growth rates are less than 10^{-6} mm/cycle. Close to the threshold ΔK_o, measured propagation rates become less than a lattice spacing per cycle, indicating that crack growth is not occurring uniformly over the entire crack front. Considering first results for quenched and tempered material at R = 0.05 (Fig. 4), it is apparent that tempering temperature exerts a strong influence on threshold values and on near-threshold crack

propagation rates. At $\Delta K = 9$ MPa$\sqrt{m}$, for example, the growth rate in the T100 condition is over two orders of magnitude greater than in the T650 condition. As the tempering temperature is raised the threshold ΔK_o increases from 3.0 to 8.5 MPa$\sqrt{m}$, concurrent with a two-fold reduction in tensile strength. At $R = 0.70$ (Fig. 5), the same trend of increasing ΔK_o with decreased strength is still apparent but the effect is drastically reduced: ΔK_o increases from 2.3 to 3.7 for the same reduction in strength.

The variations of threshold ΔK_o with monotonic yield strength and ultimate tensile strength (U.T.S.) are plotted in Figs. 8 and 9 respectively, indicating a general trend of an inverse dependence of ΔK_o on material strength. Far better correlation with ΔK_o is obtained using the U.T.S. rather than yield stress since the three treatments tested with the same monotonic yield strength (T100, T470, and ISO250) all show different threshold ΔK_o values at $R = 0.05$ (Fig. 10). This suggests that strain hardening may be important. The flow stresses within the cyclic plastic zone generated ahead of a growing fatigue crack, however, are governed by cyclic rather than monotonic strain hardening effects. Accordingly, cyclic stress-strain tests were performed to assess cyclic yield strengths. A comparison of cyclic and monotonic stress-strain curves is shown in Fig. 11 for quenched and tempered, and isothermally transformed structures. All conditions can be seen to cyclically soften with the exception of the T100 condition which cyclically hardens, and the ISO250 condition where neither significant hardening nor softening can be observed. Utilizing this

data, a better correlation can be obtained between threshold ΔK_o and material strength (now plotted as the 0.2% offset cyclic yield stress) as shown in Fig. 12. As cyclic strength is increased, either because of high initial monotonic strength or by cyclic hardening, the threshold for fatigue crack propagation is reduced, to a limiting value of ΔK_o = 3.0 MPa$\sqrt{m}$ at a yield of 1600 MPa for R = 0.05, and 2.3 MPa$\sqrt{m}$ at a yield of 1200 MPa at R = 0.70. At greater yield strengths, no further reduction in ΔK_o can be measured in this steel. It is now reasonable to expect why the three structures with identical monotonic yield strengths (i.e., T100, T470, and ISO250) show widely differing values of ΔK_o. The T100 condition has the smallest threshold because this structure is the hardest, due to cyclic hardening. The T470 condition, on the other hand, is the softest condition after cyclic softening, and consequently has the largest threshold.

Figure 12 also indicates that the effect of load ratio (mean stress) on ΔK_o becomes more pronounced as strength is reduced. Furthermore, unlike the high growth rate regime C, microstructural influences on the propagation rate are most pronounced at low mean stress (R = 0.05) and largely disappear at R = 0.70. This is shown in Fig. 13, where the variation of threshold ΔK_o with load ratio is plotted for the various microstructures tested. Whereas large differences in ΔK_o for different structures are observed at R = 0.05, at R = 0.70 the threshold value for most conditions is approximately 2.3 MPa$\sqrt{m}$.

Fracture morphology of near-threshold fatigue failure consisted of a flat, ductile transgranular mode (Fig. 14a) which was finer (yet otherwise similar) in appearance to low magnification pictures of fractures in the mid-growth rate range. Striations, however, could not be resolved. Segments of intergranular fracture (Fig. 14) were also observed, the proportion of which depended critically on the stress intensity. At low ΔK values close to ΔK_o, the amount of intergranular fracture was small (<1%), rising to a maximum at around ΔK = 6-10 MPa$\sqrt{m}$, and then gradually diminishing at higher stress intensities (Fig. 14b-d). Furthermore, the contribution from intergranular fracture was different for different tempering treatments. Significant amounts of intergranular facets could be seen in the T100 and T470 conditions, typically 15% at ΔK = 7 MPa$\sqrt{m}$, compared to a maximum of 8% in the T300 condition, and none at all in the T650 structure. A more detailed analysis of near-threshold fatigue fracture morphology in this steel is presented elsewhere [17].

In contrast to growth at higher stress intensities [5], there is little evidence in the present study to suggest that the occurrence of intergranular fracture results in lower near-threshold fatigue crack propagation resistance. Improved resistance to such propagation is not necessarily brought about by mechanism change but achieved, instead, by the utilization of cyclically softer material.

DISCUSSION

The present results have confirmed that microstructure and load ratio effects on fatigue crack propagation in steels occur primarily at high and low growth rates. The mid-range of growth rates, where the crack growth rate curve is linear, has been associated with a ductile striation mechanism of growth, with the exponent 'm' in Eq. (1). found to lie between 2.5 - 2.7. This is consistent with most metallurgical [3] and mechanical models [18-20] of "ductile" fatigue crack growth which predict an exponent of approximately 2. Such models also predict little influence of load ratio and microstructure on growth rates, and this is clearly verified by the present results in this region. Where the mechanism of failure is ductile striations, fatigue crack growth appears to be controlled by the amount of crack opening each cycle, dependent upon the elastic modulus.

At high growth rates (regime C), the present results show i) an acceleration in growth rate, ii) increased values of the exponent 'm'. iii) large microstructure effects and iv) a marked influence of load ratio. This behavior has been previously characterized in terms of the occurrence of static fracture modes [5,6], and such mechanisms have been observed in this region in the present study (Fig. 7). The microstructural influences on growth rate arise here because such static fracture mechanisms are sensitive to material inhomogenities, which control the toughness. An influence of load ratio is observed because cleavage and intergranular cracking are largely tensile stress-controlled fracture modes and fibrous fracture is dependent on the

hydrostatic component of stress. Increasing the load ratio raises K_{max} with respect to ΔK, and therefore leads to an increased contribution from such mechanisms. Thus, the onset of an acceleration in growth rate in region C is essentially a function of the toughness, brought about as K_{max} approaches K_{Ic}.

At low growth rates, less the 10^{-6} mm/cycle in region A, fatigue crack growth similarly becomes markedly sensitive to load ratio and microstructure. It is tempting to relate this again to a fracture mechanism change [4], i.e. the occurrence of intergranular cracking at low values of ΔK (Fig. 14). However, the lack of such features in the T650 condition (which shows the largest load ratio effect) and the fact that less intergranular fracture can be observed at high load ratios [17] suggests that this is an oversimplication. It is believed that the occurrence of intergranular cracking in this region is due to the influence of water vapor in air environment, causing hydrogen to diffuse to and embrittle prior austenite grain boundaries, particularly when the plasticity is confined within a single grain. Cooke, et al. [7] have shown that by testing a similar steel *in vacuo* the intergranular fracture largely disappears. Furthermore, the lack of intergranular cracking in the T650 condition is consistent with the fact that this condition is far less sensitive to hydrogen embrittlement [21]. The observation that the overall proportion of grain boundary facets changes with tempering temperature suggests a further influence of the grain boundary strength, which would depend on any impurity segregation there. It has been shown, for example, that by step-cooling 300-M

steel after tempering at 650°C, to allow silicon and phosphorus segregation to grain boundaries (temper embrittlement), the threshold ΔK_o for fatigue crack propagation in humid air is reduced by 27-28% [22]. There is clearly a close interrelationship here between the sensitivity of the material to the environment (i.e. hydrogen embrittlement from moisture in air) and to any impurity segregation to grain boundaries (i.e. temper embrittlement or tempered martensite embrittlement) which determines the amount of intergranular cracking observed during near-threshold fatigue crack growth.

The most important finding of this study is the dependence of near-threshold fatigue crack propagation rates and the value of the threshold ΔK_o on material strength, since no such dependence has been observed at higher growth rates. Examination of the literature (Fig. 15) indicates that this trend of increasing ΔK_o with decreasing strength clearly exists for steels. Kitagawa, et al [23] and Masounave and Baïlon [11] have observed similar effects in much lower strength steels. The present work has shown that such a relationship exists for ultra-high strength steels, provided that cyclic strength is considered rather than the monotonic yield stress. Consequently, cyclic softening must be regarded as beneficial in improving near-threshold crack growth resistance. Cyclic softening in quenched and tempered steels is generally attributed to a rearrangement of dislocaton substructure substructure and a reduction in dislocation density with alternating loading [24]. Cyclic hardening, on the other hand, has been attributed to dynamic strain aging and is characteristic of untempered and lightly

tempered steel having high dislocation densities [24]. Such hardening is not beneficial to near-threshold crack growth resistance, as shown by the T100 condition which displayed the lowest threshold ΔK_o value measured in 300-M steel. The isothermally transformed structure (ISO250) shows no significant hardening or softening with respect to the monotonic properties. It is worth noting that this structure contains 12% retained austenite, and the absence of cyclic softening can be considered to result from a counterbalance between softening due to dislocation rearrangement (characteristic of the 300°C temper), and hardening due to strain-induced transformation of retained austenite to martensite. Such hardening is apparent under monotonic loading in the form of increased ultimate tensile strength (compare T470 with ISO250), as shown in Fig. 16, where the stability of retained austenite with respect to strain is plotted for the T100, T300, T470 and ISO250 conditions. Transformation-induced hardening will not be significant in quenched and tempered structures because less than 2% retained austenite remains after yield (Fig. 16). The ISO250 structure has also been shown to exhibit markedly improved stress corrosion cracking resistance in distilled water [25] when compared to quenched and tempered 300-M at the same (monotonic) yield strength (T470 condition). Since the mechanisms of stress corrosion cracking in water in this steel are thought to be similar to the mechanisms of environmental attack during fatigue crack growth in humid air (i.e. hydrogen embrittlement arising from the presence of water vapor [26]), this structure might be expected to show improved near-threshold fatigue

crack growth resistance with respect to the T470 condition. This, in fact, is not observed under cyclic conditions (Fig. 10) because the ISO250 structure does not cyclically soften and, therefore, is cyclically harder than the T470 condition. When compared at the same cyclic yield stress, however, the ISO250 condition does show marginally superior threshold values compared to quenched and tempered material (Fig. 12).

Although it is clear from the present results in steels that, for low growth rates less than 10^{-6} mm/cycle, fatigue crack propagation in humid air is sensitive to microstructure and mean stress (load ratio), the reason for this behavior is not immediately apparent. Any explanation must take account of the observations that increased crack growth rates and a lower threshold ΔK_o occur 1) when the load ratio (R) is increased, particularly for lower strength material (mean stress effect), and 2) when the cyclic yield strength of the steel is decreased, particularly for low load ratios (microstructure effect). We now discuss possible mechanisms for these effects.

i) Crack Closure

Elber [27] has suggested that, due to residual compressive stresses generated from permanent tensile deformation left in the wake of a growing fatigue crack, partial closure of crack surfaces may occur at positive loads during a tension-tension cycle. This closure effectively limits the actual alternating stress intensity (ΔK) experienced in the vicinity of the crack tip, since the crack cannot propagate while it is closed. At high load ratios, however, the crack

remains open for a larger portion of each cycle, and thus the reduction in applied ΔK[1] from closure is less significant. This model, therefore, provides an explanation for increased near-threshold growth rates at higher load ratios [9,10], but does not indicate why this mean stress effect diminishes at faster propagation rates (regime B), where closure is just as likely to occur. One can postulate that the influence of cyclic strength also follows from closure, since, in lower strength materials, larger plastic zones are created ahead of the crack tip, and hence residual stresses arising from crack closure, may be more effective in retarding growth over larger distances. Electrical potential measurements during the present investigation, however, failed to detect any closure near the threshold, except below the minimum stress intensity (K_{min}) of the loading cycle. This lends support to previous observations [28] of a negligible effect from crack closure for crack growth under plane strain conditions. The electrical potential technique, however, for monitoring contact of fracture surfaces cannot be regarded as totally satisfactory, since in air, surfaces are likely to be coated with oxide scale.

ii) Environmental Influence

The effect of load ratio and microstructure on fatigue crack propagation at low stress intensities can also be rationalized in terms of the environmental influence of hydrogen from moist air (hydrogen embrittlement). This can occur under fatigue loading at stress intensities less than the threshold for hydrogen-assisted cracking under monotonic loading (K_{TH}) because fresh surface at the crack tip,

[1] Applied ΔK refers to the value of ΔK calculated from a knowledge of applied loads and crack length.

where molecular hydrogen can adsorb and dissociate, is continually renewed by cyclic stressing. Specifically, hydrogen atoms are considered to diffuse to the region of maximum hydrostatic tension ahead of the crack tip, thereby lowering the cohesive strength of the lattice [29]. Increased fatigue crack growth rates in steels would be expected by increasing the load ratio, since the higher value of K_{max} creates a larger stress gradient to promote hydrogen transport. Furthermore, higher propagation rates should be seen in harder material because the increased strength can lead to a larger equilibrium solubility of hydrogen ahead of the crack tip (due to higher triaxiality), and a reduction in the amount of hydrogen necessary to cause cracking. This is reflected under monotonic loading in an increasing susceptibility to hydrogen embrittlement as the yield strength is raised [21]. Thus, if hydrogen embrittlement is considered to be an important contribution to the cracking of steels under cyclic loading in moist air, higher near-threshold growth rates and a lower threshold ΔK_o would be predicted as the strength and load ratio is increased, as has been experimentally observed. Furthermore, this argument is consistant with i) the absence of an influence of load ratio on propagation rates for steels tested under vacuum [7], and ii) the absence of load ratio and strength effects at higher (regime B) growth rates since, at higher crack velocities, there would be insufficient time for the permeation of atomic hydrogen into the crack tip region.

It is not possible from the present investigation to decipher which mechanism is primarily responsible for the influence of mean

stress and cyclic strength on low (near-threshold) growth rates, but it is plausible that both effects are contributing. Crack closure arguments, however, are less convincing because they do not explain why the influences of load ratio and strength are not observed in regime B, and why the load ratio effect at low growth rates disappears for tests *in vacuo*. Fatigue testing steels of differing strength under vacuum would provide one critical experiment to resolve this issue. In the absence of such data a semi-quantitative model is now developed for the threshold for fatigue crack growth in steels, based on the influence of hydrogen from the environment on near-threshold fatigue crack propagation.

Model for the Fatigue Crack Growth Threshold in Steels

For near-threshold fatigue crack propagation in the absence of an environment we adopt a critical fracture stress criterion for crack growth. Following Weiss and Lal [30], the crack advance per cycle (da/dN) can be considered to extend over a distance (equated to a critically stressed volume) over which the nominal stress exceeds a certain critical fracture stress (σ_F), such that

$$\frac{da}{dN} = a\left(\frac{\Delta\sigma_N}{\sigma_F}\right)^{\frac{n_F+1}{n_F}} \cdot f(\tfrac{a}{w}) - \rho_*/2 \ , \qquad (2)$$

where a is the crack length, $\Delta\sigma_N$ the applied stress amplitude, $f(\frac{a}{w})$ a dimensionless correction factor for the finite width of specimens, n_F the cyclic strain hardening exponent in the stress range to which the critically stressed region is subjected, and ρ_* the Neuber

microsupport constant, representing the effective radius of a sharp crack. For near-threshold fatigue crack growth, the maximum cyclic stress decreases towards the elastic limit, hence n_F must approach unity. Thus, it follows that

$$\frac{da}{dN} = \frac{\Delta K^2}{\pi \sigma_F^2} - \frac{\rho_*}{2} \quad , \tag{3}$$

where

$$\Delta K^2 = \pi a \cdot \Delta \sigma_N^2 \cdot f(\tfrac{a}{w}) \ .$$

For crack growth, the local tensile stress (σ_{yy}) must exceed σ_F over a distance larger than ρ_*, and thus, at the threshold, Weiss and Lal [30] suggest $da/dN = \rho_*$, viz

$$\Delta K_o = \sqrt{\frac{3}{2} \pi \rho_*} \cdot \sigma_F \ . \tag{4}$$

In the presence of an aqueous or gaseous environment, hydrogen atoms can be adsorbed on freshly exposed metal surface at the crack tip by one of the following mechanisms:

i) in water vapor: $2H^+ + 2e \rightleftharpoons 2H$ (at cathodic sites),

ii) in gaseous hydrogen: $H_{2(gas)} \rightleftharpoons H_{2(surface)} \rightleftharpoons 2H$ (at exposed surface),

iii) in hydrogen sulfide: $H_2S + Fe \rightleftharpoons FeS + 2H$ (at exposed surface).

The plastic stress gradient ahead of the crack tip then provides the driving force for diffusion of atomic hydrogen into the region of highest dilatation (ie. maximum hydrostatic tension), resulting in a reduction in the cohesive strength [29]. Thus, in the presence of an

environment, we can write

$$\Delta K_o = \sqrt{\frac{3}{2}\pi\rho_*} \cdot (\sigma_F - \Delta\sigma_H) \ , \qquad (5)$$

where $\Delta\sigma_H$ is the reduction in cohesive strength due to hydrogen. Following Oriani and Josephic [31], we assume that $\Delta\sigma_H$ is proportional to the local concentration of hydrogen at the point of highest triaxial tension (C_H), and that this concentration at equilibrium can be obtained from

$$\Delta\sigma_H = \alpha C_H = \alpha C_o \exp\left(\frac{\bar{\sigma} \cdot \bar{V}}{R_o T}\right) \ , \qquad (6)$$

where C_o is the equilibrium concentration of hydrogen in the unstressed lattice, α an unknown constant, $\bar{V}$ the partial molar volume of hydrogen in iron (2 cm^3/mole), $\bar{\sigma}$ the hydrostatic tension, R_o the gas constant and T the absolute temperature. Combining Eqs. (5) and (6), we have

$$\Delta K_o = \sqrt{\frac{3}{2}\pi\rho^*} \cdot \left[\sigma_F - \alpha C_o \exp\left(\frac{\bar{\sigma} \cdot \bar{V}}{R_o T}\right)\right] \ . \qquad (7)$$

The hydrostatic tension ($\bar{\sigma}$) is defined as the mean of the three principal stresses ahead of the crack tip (σ_{xx}, σ_{yy}, σ_{zz}), and can be approximated under conditions of plastic flow using Hill's slip-line field equations for plane strain, ie.

$$\bar{\sigma} = \frac{1}{3}(\sigma_{xx} + \sigma_{yy} + \sigma_{zz}) = \alpha_1 \sigma_y \ln\left[\left(1+\frac{x}{\rho}\right) + \frac{1}{2}\right] \ , \qquad (8)$$

where σ_y is the yield strength, x the distance ahead of the crack tip, ρ the crack tip radius and α_1 a coefficient (>1) allowing for an increase in plastic constraint due to work hardening. Rewriting Eq. (8) in terms of the plastic constraint factor ($\sigma_{yy}^{max}/\sigma_y$) ahead of the crack tip [21], it follows that $\bar{\sigma}$ can be approximated by

$$\bar{\sigma} = \alpha_1 (\sigma_{yy}^{max}/\sigma_y - \frac{1}{2}) \simeq \sigma_y + 2\alpha_2 K \quad , \tag{9}$$

where $\sigma_{yy}^{max}/\sigma_y \simeq 1 + \alpha_2(K/\sigma_y)$.[1] K is the stress intensity, α_2 an empirical constant = 2 $in^{-1/2}$, and α_1 is taken to be equal to 2. Combining Eqs. (7) and (9) and putting $K = K_{max} = \Delta K/1-R$, where $R = K_{min}/K_{max}$, we have

$$\Delta K_o \simeq \sqrt{\frac{3}{2}\pi\rho_*} \cdot \left\{\sigma_F - \alpha C_o \exp\left[\frac{\bar{V}}{R_o T}\left(\sigma_y + \frac{2\alpha_2 \Delta K_o}{1-R}\right)\right]\right\} . \tag{10}$$

Rearranging Eq. (10), assuming $\frac{\bar{V}\,\alpha_2\,\Delta K_o}{R_o T\,(1-R)}$ is small, gives

$$\Delta K_o \simeq \sqrt{\frac{3}{2}\pi\rho_*} \left[\frac{\sigma_F - \alpha C_o \exp(B\sigma_y)}{1 + \frac{\alpha C_o \cdot \rho_*^{1/2}}{(1-R)} \cdot B' \cdot \exp(B\sigma_y)}\right] , \tag{11}$$

where $B = \bar{V}/R_o T$, and $B' = \sqrt{\frac{3}{2}\pi} \cdot \frac{\bar{V}}{R_o T} \cdot 2\alpha_2$. At ambient temperature, $B = 8 \times 10^{-4}$ $(MPa)^{-1}$, and $B' = 5 \times 10^{-2}$ $(MPa\sqrt{m})^{-1}$.

---

[1] This expression for the plastic constraint factor was first observed by Hahn and Rosenfield [32] for mild steel, but recent studies [33] have shown that it is also valid for high strength low alloy steels such as 4340.

Evaluation of the remaining parameters in Eq. (11) is complex. The constant α from Eq. (8) is unknown at this time, requiring experimental measurement. Furthermore, the significance of σ_F and $\rho*$ at the threshold is also uncertain. σ_F represents the critical fracture stress in the absence of environmental influence, and it has been suggested [30] that, at the threshold, this stress approaches the theoretical cohesive strength ($\sigma_c \simeq$ 1/10 elastic modulus) acting across a distance ahead of the crack tip of $\rho* \sim s_o$, where s_o is the cube root of the defect-free volume. For the present steel, assuming average dislocation densities at the crack tip between $10^{12} - 10^{10}$ /cm^2, s_o (and hence ρ_*) should be of the order of 100-1000 Å. Finally, the magnitude of C_o will depend on whether the hydrogen is internal (from charging experiments) or external as hydrogen gas or from moisture. For an external gas, C_o is the hydrogen concentration in the unstressed lattice in equilibrium with a hydrogen gas pressure of P_{H_2}, which according to Sievert's Law [31] is given by

$$C_o = \beta S_L P_{H_2}^{1/2} \quad , \tag{12}$$

where S_L is Sievert's parameter for H in α-Fe = 1.26×10^9 atom H/atom Fe $(\text{torr})^{-1/2}$ and β is a multiplicative factor ($\gg 1$), which allows for the fact that the hydrogen solubility in the grain boundaries, where the fractures often occur, may be considerably larger than in the normal lattice. Again the magnitude of C_o remains unclear because of the uncertainty in the value of β. However, the form of Eq. (11) does provide a useful rationalization of fatigue threshold behavior

in steels. Firstly, any increase in the hydrostatic tension ($\bar{\sigma}$) will markedly increase the local concentration of hydrogen and hence lower the threshold (Eq. 7). This is achieved by i) raising the yield stress and ii) increasing K_{max} or the load ratio R (Eq. 10). Both effects have been experimentally observed in the present investigation (Figs. 13 and 15). Furthermore, at high yield strengths, the σ_y term in the expression for $\bar{\sigma}$ (Eq. 9) dominates the K_{max} term, suggesting a smaller load ratio effect than at low strengths where the σ_y and K_{max} terms are more comparible. This again is experimentally observed in that the influence of load ratio on ΔK_o increases as the strength decreases (Fig. 12). Moreover, since the effect of load ratio (ie. K_{max}) arises from the environmental contribution, in the absence of an environment (ie. $P_{H_2} \propto C_o = 0$), the value of ΔK_o should be unaffected by the load ratio. This is entirely consistent with existing near-threshold data for low-alloy steels [7], where the influence of load ratio on ΔK_o, measured in air, was found to disappear when tests were performed in a vacuum. Apparently, increasing the load ratio, and hence K_{max}, results in i) a larger hydrostatic tension, and ii) a larger stress gradient to aid hydrogen diffusion. If crack closure effects are considered, however, some influence of load ratio might be expected even *in vacuo*. There is a further possibility that ρ_* may be somewhat related to the yield strength, through changes in the dislocation density, for example. In this instance the value of ΔK_o would be sensitive to material strength in the absence of hydrogen effects. However, data showing the dependence of ΔK_o on yield strength for

tests in vacuum are not available at this time. Finally, increasing C_o by, for example, raising the hydrogen gas pressure, would be expected to give rise to lower threshold values, particularly for higher strength steels, and although such data are again unavailable, this is not an unexpected result.

Utilizing the model to quantitatively predict the dependence of ΔK_o on material strength requires assigning values to two parameters in Eq. (11), namely ρ_* which has been given some physical significance in terms of the defect-free volume [30], and (α C_o) which must be fitted empirically. Considering threshold data for steels ranging in strength from 200 to 2000 MPa, best fit was obtained with (α C_o) = 3.5×10^3 MPa. Using this value, with σ_F equated to the theoretical strength, the variation of ΔK_o with yield strength from Eq. (11) is shown by the solid lines in Fig. 15. It can be seen that the experimentally observed trend is correctly reproduced with all threshold values for steels lying within the curves for ρ_* = 300 and 1500 Å, which is reasonable considering the approximate nature of the estimate for $\bar{\sigma}$ (Eq. 9). The values of ρ_* are somewhat large, but still of the same order as those discussed by Weiss and Lal [30] for the threshold range. Although Eq. (11) predicts thresholds as a function of yield strength, further experimental data are required before the model can be assessed with respect to mean stress effects and the nature of the environment.

CLOSING REMARKS

It has been experimentally established that the influences of microstructure and mean stress on fatigue crack growth in steels are primarily localized to specific growth rates regimes, namely at very low and very high propagation rates. The wisdom of studying these effects over a narrow range of growth rates (ie. less than 2-3 orders of magnitude), as has been the practice in most investigations, is thus questioned because the extremes of growth rate behavior are often missed. With regard to low growth rate behavior, large effects of microstructure and mean stress on the propagation rate and on threshold values have been observed, and modeled in terms of the influence of hydrogen from water vapor in moist air. It has been found that superior resistance to near-threshold fatigue crack growth can be achieved in steels by the use of lower strength material. From a material selection viewpoint, however, it may not always be desirable to replace existing materials with others of lower strength. In this instance, optimum strength and resistance to high cycle fatigue crack growth requirements can be met by the use of materials with high monotonic strength, which significantly soften under cyclic loading. In this regard, it is perhaps interesting to note that as the tensile strength of steel is raised, the threshold (ΔK_o) for crack propagation <u>decreases</u>, and yet it is widely accepted that the fatigue endurance limit will <u>increase</u>. The threshold, however, is a measure of the minimum stress for crack <u>propagation</u> from a pre-existing crack, whereas the fatigue limit represents the minimum stress to cause crack <u>initiation</u>, propagation

and failure in an unnotched specimen. In the latter case, fatigue crack initiation can occupy more than 90% of the life where the fatigue endurance exceeds around 10^4 cycles. Since the mechanism of initiation is thought to be governed by microplastic flow, dependent on some cumulative plastic strain [30,34], it is not unreasonable to expect initiation to occur more readily in a softer material, thus reducing the fatigue limit. In fact, it has been shown that the minimum value of the stress intensity for fatigue crack initiation in HY-130 steel decreases as the yield strength is lowered [35]. Furthermore, when fatigue limits are measured in notched specimens, higher strength steels are no longer superior, because of their greater notch sensitivity [36].

CONCLUSIONS

From a study of fatigue crack propagation in 300-M ultra-high strength steel tested in humid air, the following conclusions can be made:

1. For the mid-range of growth rates (region B, Fig. 1), variations in microstructure and mean stress (load ratio) do not lead to significant changes in the crack propagation rate. The exponent 'm' in Eq. (1) was found to be between 2.5-2.7, consistent with the ductile striation mechanism of growth observed.
2. At high growth rates (region C, Fig. 1), crack propagation rates become sensitive to microstructure and load ratio consistent with the occurrence of "static" fracture modes during straition growth. Optimum fatigue cracking resistance in the region is achieved with high toughness materials.

3. At low growth rates (regime A, Fig. 1), significant effects of load ratio and microstructure on the crack propagation rates are observed; the maximum sensitivity to load ratio occurring in lower strength material, and the maximum sensitivity to microstructure occurring at low load ratios.
4. Increased near-threshold crack growth rates and a decrease in the threshold for crack propagation (ΔK_o) are seen as the load ratio (R) is increased, the value of ΔK_o being inversely related to R.
5. Increased near-threshold crack growth rates are seen as the strength of the steel is increased, the value of ΔK_o being inversely related to the cyclic yield strength. Cyclic softening (and the use of low strength steels) can thus be regarded as beneficial in improving resistance to very high cycle, low growth rate ($< 10^{-6}$ mm/cycle) fatigue crack propagation.
6. A model for the threshold (ΔK_o), for fatigue crack growth in steels, is developed based on a critical stress criterion for growth modified by the presence of hydrogen from the environment. The model can be used to rationalize the experimentally observed trends of load ratio and material strength on the value of ΔK_o.

ACKNOWLEDGEMENTS

The research was conducted under the auspices of the U.S. Energy Research and Development Administration through the Materials and Molecular Research Division of the Lawrence Berkeley Laboratory, University of California. The author would like to thank the Miller Institute for Basic Research in Science for the award of a University Miller Research Fellowship, Professors E. R. Parker and V. F. Zackay for their constant support and encouragement, and Dr. R. M. Horn and Mr. J. A. Wert for helpful discussions.

REFERENCES

1. Paris, P.C., and Erdogan, F., "A Critical Analysis of Crack Propagation Laws", Journal of Basic Engineering, Transactions of the American Society of Mechanical Engineers, Series D., Vol. 85, Dec. 1963, pp. 528-539.

2. Heaton, M.D., "Application of Fracture Mechanics to Power Plant", Proceedings of Conference on "The Mechanics and Physics of Fracture," Cambridge, U.K., Jan. 1975. (The Institute of Physics/The Metals Society, London).

3. Pelloux, R.M.N., "Crack Extension by Alternating Shear", Engineering Fracture Mechanics, Vol. 1., No. 4, April 1970, pp. 697-704.

4. Richards, C.E. and Lindley, T.C., "The Influence of Stress Intensity and Microstructure on Fatigue Crack Propagation in Ferritic Materials", Engineering Fracture Mechanics, Vol. 4, No. 4, Dec. 1972, pp. 951-978.

5. Ritchie, R.O. and Knott, J.F., "Mechanisms of Fatigue Crack Growth in Low Alloy Steel", Acta Metallurgica, Vol. 21, No. 5, May 1973, pp. 639-648.

6. Ritchie, R.O. and Knott, J.F., "Micro Cleavage Cracking During Fatigue Crack Propagation in Low Strength Steel", Materials Science and Engineering, Vol. 14, No. 1, April 1974, pp. 7-14.

7. Cooke, R.J., Irving, P.E., Booth, G.S., and Beevers, C.J., "The Slow Fatigue Crack Growth and Threshold Behaviour of a Medium Carbon Alloy Steel in Air and Vacuum", Engineering Fracture Mechanics, Vol. 7, No. 1, March 1975, pp. 69-77.

8. Robinson, J.L., Irving, P.E., and Beevers, C.J., "An Analytic Approach to Low Stress Fatigue Crack Growth in Titanium", Proceedings of Third International Congress on Fracture, Munich, W. Germany, April 1973, Vol. V, Paper V-343. (Verein Deutscher Eisenhüttenleute, Düsseldorf).

9. Paris, P.C., Bucci, R.J., Wessel, E.T., Clark, W.G., and Mager, T.R., "Extensive Study of Low Fatigue Crack Growth Rates in A533 and A508 Steels", Stress Analysis and Growth of Cracks, ASTM STP 513, American Society for Testing and Materials, 1972, pp. 141-176.

10. Schmidt, R.A., and Paris, P.C., "Threshold for Fatigue Crack Propagation and the Effects of Load Ratio and Frequency", Progress in Flaw Growth and Fracture Toughness Testing, ASTM STP 536, American Society for Testing and Materials, 1973, pp. 79-94.

11. Masounave, J., and Baïlon, J-P., "Effects of Grain Size on the Threshold Stress Intensity Factor in Fatigue of a Ferritic Steel," Scripta Metallurgica, Vol. 10, No. 2, Feb. 1976, pp. 165-170.

12. Ritchie, R.O., "Effects of Strength and Grain Size on Near-Threshold Fatigue Crack Growth in Ultra-high Strength Steel", Proceedings of Fourth International Conference on Fracture, Waterloo, Canada, June 1977. (Lawrence Berkeley Laboratory, Report No. LBL-5188, June 1976, University of California).

13. Ritchie, R.O., Garrett, G.G., and Knott, J.F., "Crack Growth Monitoring: Optimization of the Electrical Potential Technique Using an Analogue Method", International Journal of Fracture Mechanics, Vol. 7, No. 4, Dec. 1971, pp. 462-467.

14. Bhandarkar, D., Zackay, V. F., and Parker, E.R., "Stability and Mechanical Properties of Some Metastable Austenitic Steels", Metallurgical Transactions, Vol. 3, No. 10, Oct. 1972, pp. 2619-2631.

15. Landgraf, R.W., Morrow, J-D., and Endo, T., "Determination of the Cyclic Stress-Strain Curve", Journal of Materials, Vol. 4, No. 1., 1969, pp. 176-188.

16. Witt, F.J., "Equivalent Energy Procedures for Predicting Gross Plastic Fracture", Fourth National Symposium on Fracture Mechanics, Carnegie Mellon University, Aug. 1970.

17. Ritchie, R.O., "Fractography of Fatigue Crack Propagation in 300-M Alloy Steel", Metallurgical Transactions A, to be published. (Lawrence Berkeley Laboratory Report No. LBL-5497, Nov. 1976, University of California).

18. Liu, H.W., "Fatigue Crack Propagation and Applied Stress Range - An Energy Approach", Journal of Basic Engineering, Transactions of the American Society of Mechanical Engineers, Series D, Vol. 85, 1963, pp. 116-120.

19. Antolovich, S.D., Saxena, A., and Chanani, G.R., "A Model for Fatigue Crack Propagation", Engineering Fracture Mechanics, Vol. 7, No. 4, 1975, pp. 649-652.

20. Purushothaman, S., and Tien, J.K., "A Fatigue Crack Growth Mechanism for Ductile Materials", Scripta Metallurgica, Vol. 9, 1975, pp. 923-926.

21. Gerberich, W.W., and Chen, Y.T., "Hydrogen-Controlled Cracking - An Approach to Threshold Stress Intensity", Metallurgical Transactions A, Vol. 6A, No. 2, Feb. 1975, pp. 271-278.

22. Ritchie, R.O., "Influence of Impurity Segregation on Temper Embrittlement and on Slow Fatigue Crack Growth and Threshold Behavior in 300-M High Strength Steel", Metallurgical Transactions A, to be published. (Lawrence Berkeley Laboratory Report No. LBL-5498, Oct. 1976, University of California).

23. Kitagawa, H., Nishitani, H., and Matsumoto, J., "Fracture Mechanics Approach to Threshold Condition for Fatigue Crack Growth", Proceedings of Third International Congress on Fracture, Munich, W. Germany, April 1973, Vol. 5, Paper V-444/A. (Verein Deutscher Eigenhüttenleute, Düsseldorf).

24. Thielen, P.N., Fine, M.F., and Fournelle, R.A., "Cyclic Stress Strain Relations and Strain-Controlled Fatigue of 4140 Steel," Acta Metallurgica, Vol. 24, No. 1, Jan. 1976, pp. 1-10.

25. Ritchie, R.O., Castro-Cedeno, M.H., Parker, E.R., and Zackay, V.F., "Stress Corrosion Cracking in Ultra-high Strength Steels: Effect of Retained Austenite and Silicon Modifications to AISI 4340 Steel", Metallurgical Transactions A, to be published. (Lawrence Berkeley Laboratory Report No. LBL-5499, Nov. 1976, University of California).

26. Wei, R.P. and Landes, J.D., "Correlation between Sustained-Load and Fatigue Crack Growth in High-Strength Steels", Materials Research and Standards, MTRSA, American Society for Testing and Materials, Vol. 9, 1969, pp. 25.

27. Elber, W., "The Significance of Fatigue Crack Closure", Damage Tolerance in Aircraft Structures, ASTM STP 486, American Society for Testing and Materials, 1971, pp. 230-242.

28. Lindley, T.C., and Richards, C.E., "The Relevance of Crack Closure to Fatigue Crack Propagation", Materials Science and Engineering, Vol. 14, No. 3, June 1974, pp. 281-293.

29. Troiano, A.R., "The Role of Hydrogen and Other Interstitials in the Mechanical Behavior of Metals," Transactions of the American Society for Metals, Vol. 52, No. 1, Jan. 1960, pp. 54-80.

30. Weiss, V., and Lal, D.N., "A Note on the Threshold Condition for Fatigue Crack Propagation," Metallurgical Transactions, Vol. 5, No. 8, Aug. 1976, pp. 1946-1949.

31. Oriani, R.A. and Josephic, P.H., "Equilibrium Aspects of Hydrogen-Induced Cracking of Steels," Acta Metallurgica, Vol. 22, No. 9, Sept. 1974, pp. 1065-1074.

32. Hahn, G.T., and Rosenfield, A.R., "Experimental Determination of Plastic Constraint Ahead of a Sharp Crack Under Plane Strain Conditions," Transactions of the American Society for Metals, Vol. 59, No. 4, 1966, pp. 909-916.

33. Santhanam, A.T., "Determination of Plastic Constraint Ahead of a Sharp Crack in Ni-Cr-Mo-V and Type 4340 Steel," Proceedings of the Second International Conference on Mechanical Behavior of Materials, Boston, MA, Aug. 1976, pp. 1022-1026.

34. Jack, A.R., and Price, A.T., "The Initiation of Fatigue Cracks from Notches in Mild Steel Plates", International Journal of Fracture Mechanics, Vol. 6, No. 4, Dec. 1970, pp. 401-409.

35. Barsom, J.M., and McNicol, R.C., "Effects of Stress Concentration on Fatigue-Crack Initiation in HY-130 Steel," Fracture Toughness and Slow-Stable Cracking, ASTM STP 559, American Society for Testing and Materials, 1974, pp. 183-204.

36. Cummings, H.N., Stulen, F.B., and Schulte, W.C., "Relation of Inclusions to the Fatigue Properties of SAE 4340 Steel", Transactions of the American Society for Metals, Vol. 49, 1957, pp. 482-512.

TABLE CAPTIONS:

Table 1. Mechanical Properties (monotonic) of 300-M Steel.

FIGURE CAPTIONS:

Fig. 1. Schematic diagram showing the primary fracture mechanisms in steels associated with the sigmoidal variation of fatigue crack propagation rate (da/dN) with alternating stress intensity (ΔK). ΔK_o is the threshold stress intensity for crack growth, and K_c the stress intensity at final failure.

Fig. 2. Effect of tempering temperature on ambient temperature uniaxial tensile properties of 300-M alloy steel, oil quenched from 870°C.

Fig. 3. Effect of tempering temperature on ambient temperature plane strain fracture toughness (K_{Ic}) of 300-M alloy steel, oil quenched from 870°C.

Fig. 4. Variation of fatigue crack growth rate (da/dN) with alternating stress intensity (ΔK) at R=0.05, for 300-M steel, quenched and tempered between 100°C and 650°C.

Fig. 5. Variation of fatigue crack growth rate (da/dN) with alternating stress intensity (ΔK) at R=0.70, for 300-M steel, quenched and tempered between 100°C and 650°C.

Fig. 6. Variation of fatigue crack growth rate (da/dN) with alternating stress intensity (ΔK) at R=0.05 and 0.70, for 300-M steel isothermally transformed at 250°C (ISO250). Results are compared with 300-M steel, quenched and tempered i) at the same temperature (T300) and ii) to the same monotonic yield strength (T470).

Fig. 7. Mechanisms of growth at medium and high growth rates. a) Ductile striation growth in T300 condition at ΔK = 20 MPa$\sqrt{m}$ (R=0.05); b) Intergranular, cleavage and fibrous fracture at high growth rates in T100 condition at ΔK = 30 MPa$\sqrt{m}$ (R=0.05); and c) fibrous fracture during striation growth in T300 condition at ΔK = 60 MPa$\sqrt{m}$ (R=0.05). [S = striations, F = fibrous (micro-void coalescence), C = cleavage, I = intergranular cracking; arrow indicates general direction of crack propagation].

Fig. 8. Influence of monotonic yield strength (σ_y) on threshold for fatigue crack growth (ΔK_o) at R=0.05 and 0.70, in 300-M, tested in moist air.

Fig. 9. Influence of ultimate tensile strength (U.T.S.) on threshold for fatigue crack growth (ΔK_o) at R=0.05 and 0.70, in 300-M, tested in moist air.

Fig. 10. Comparison of fatigue crack growth behavior at R=0.05 of T100, T470 and ISO250 structures which show identical monotonic yield strength, but differing cyclic hardening/softening response.

Fig. 11. Comparison of monotonic and cyclic stress-strain curves for 300-M steel, after quench and tempering and isothermal transformation heat-treatments.

Fig. 12. Influence of cyclic yield strength ($\sigma_{y'}$), measured by 0.2% offset, on threshold for fatigue crack growth (ΔK_o) at R=0.05 and 0.70, in 300-M steel, tested in moist air.

Fig. 13. Threshold for fatigue crack growth (ΔK_o) versus load ratio ($R=K_{min}/K_{max}$), at R=0.05 and 0.70, for 300-M steel.

Fig. 14. Mechanisms of growth at low growth rates, showing ductile transgranular mechanism with segments of intergranular fracture (I), in T470 condition at R=0.05. a) & b) At threshold, ΔK = 5.2 MPa$\sqrt{m}$ (ΔK_o = 5.1 MPa$\sqrt{m}$), c) ΔK = 7.6 MPa$\sqrt{m}$, and d) ΔK = 11 MPa$\sqrt{m}$. [Arrow indicates general direction of crack propagation].

Fig. 15. Summary of results showing variation of threshold for fatigue crack growth (ΔK_o) at R=0 with yield strength for steels. Solid lines from threshold model (Eq. 11).

Fig. 16. Mechanical stability of retained austenite in quenched and tempered and isothermally transformed 300-M with respect to strain. True stress-true strain curves are plotted, superimposed with the amount of untransformed austenite. Shaded areas represent the amount of austenite transformed prior to yield (equivalent to stress-assisted transformation).

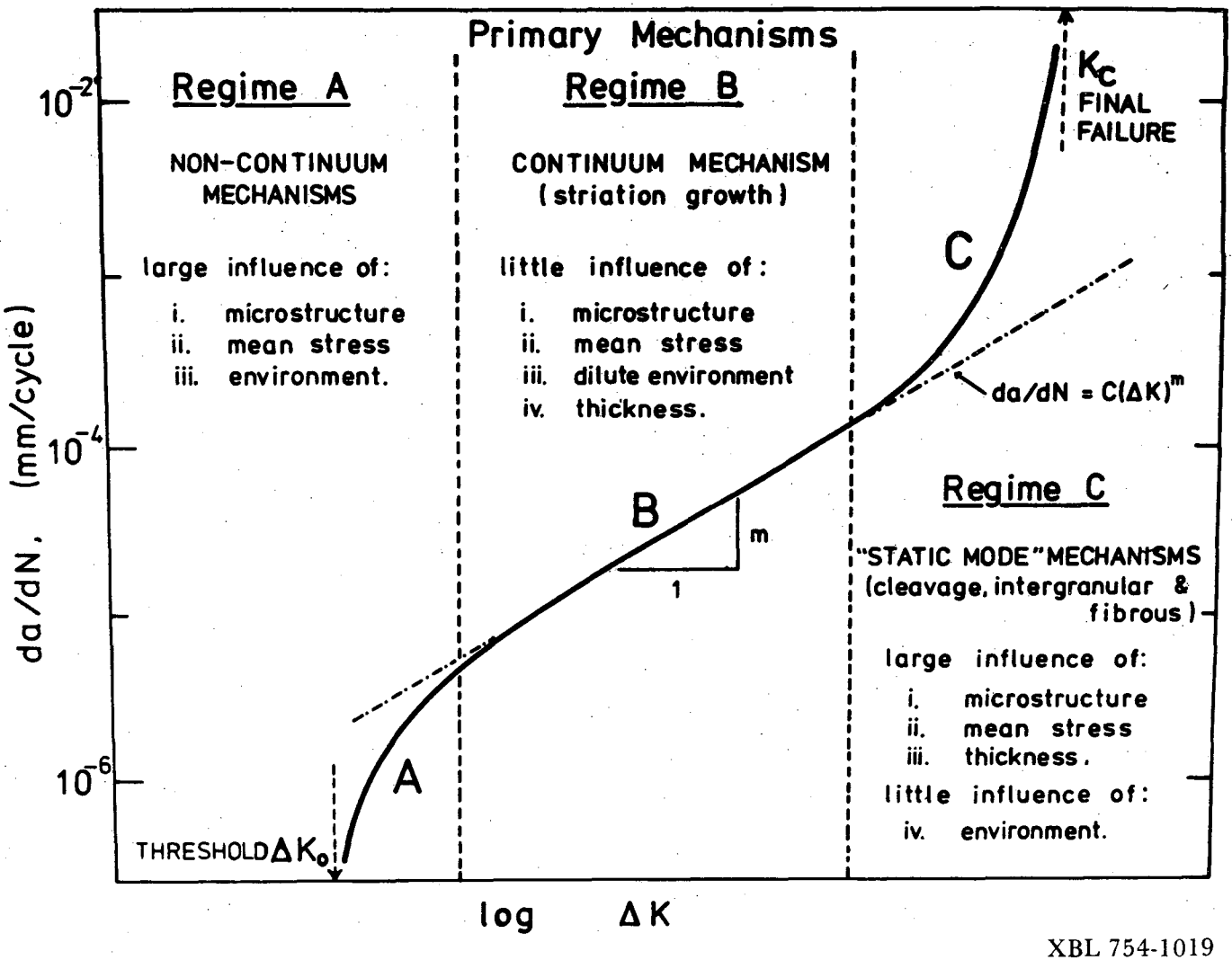

XBL 754-1019

Fig. 1. Schematic diagram showing the primary fracture mechanisms in steels associated with the sigmoidal variation of fatigue crack propagation rate (da/dN) with alternating stress intensity (ΔK). ΔK_o is the threshold stress intensity for crack growth, and K_c the stress intensity at final failure.

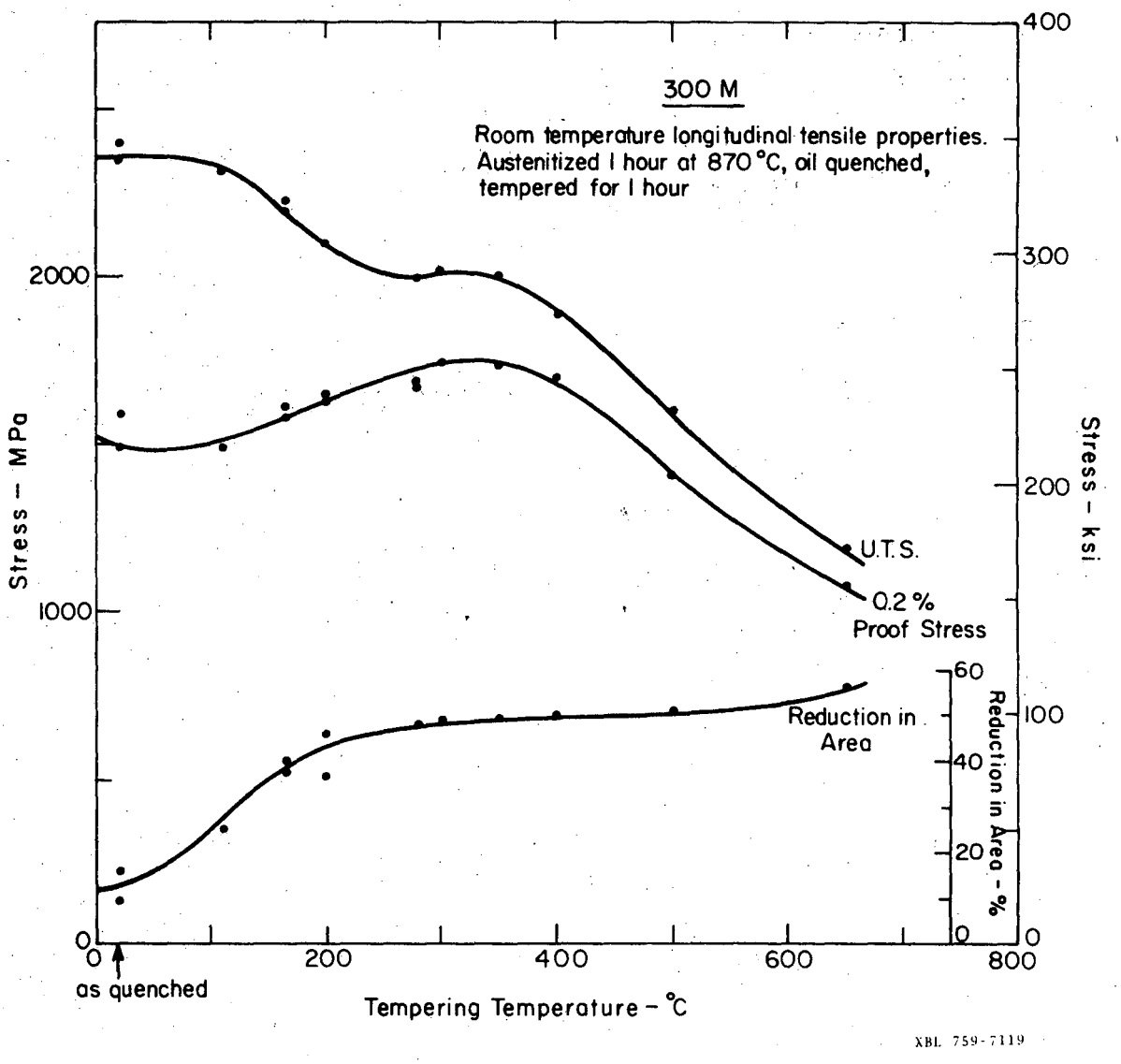

Fig. 2. Effect of tempering temperature on ambient temperature uniaxial tensile properties of 300-M alloy steel, oil quenched from 870°C.

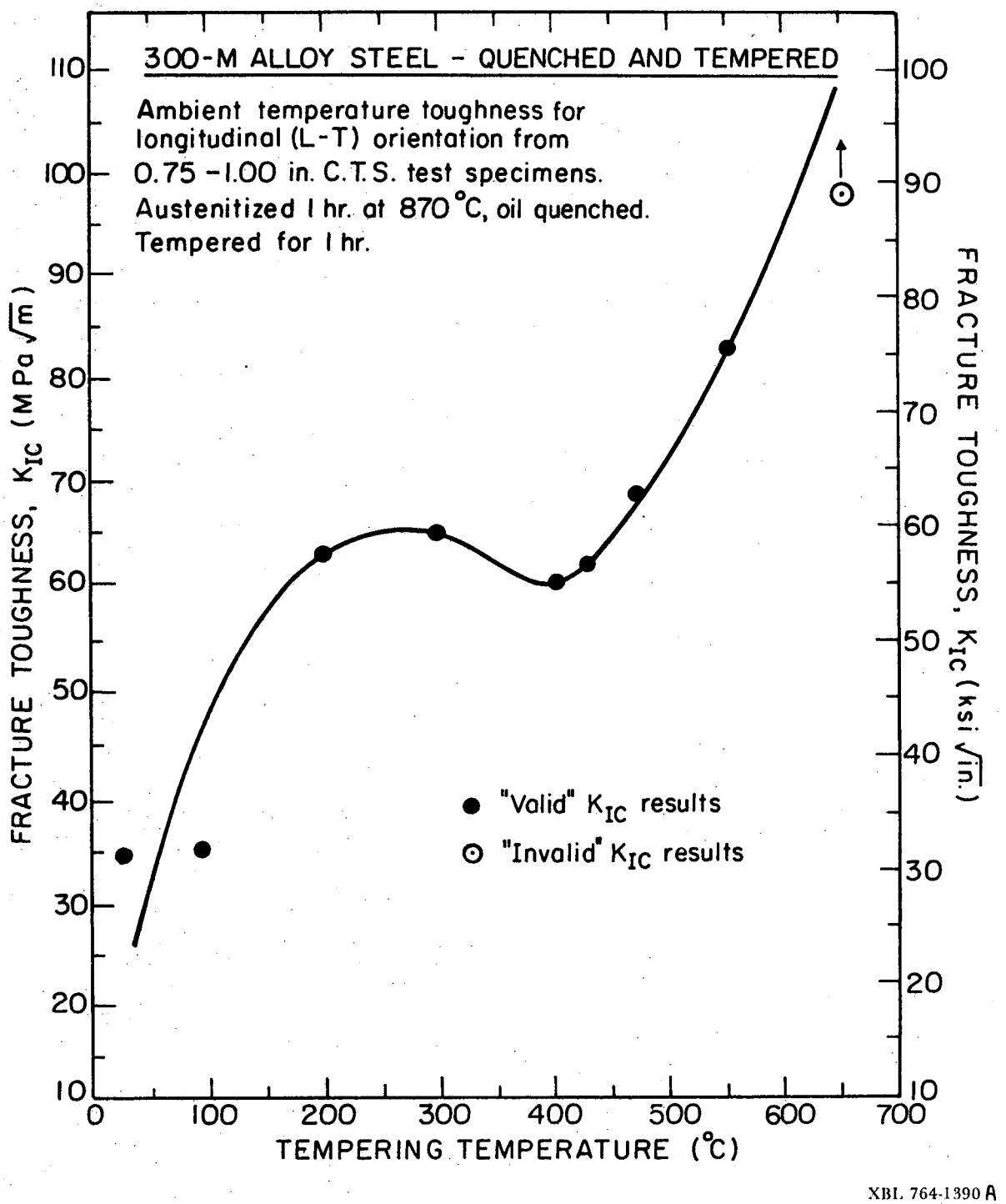

XBL 764-1390 A

Fig. 3. Effect of tempering temperature on ambient temperature plane strain fracture toughness (K_{Ic}) of 300-M alloy steel, oil quenched from 870°C.

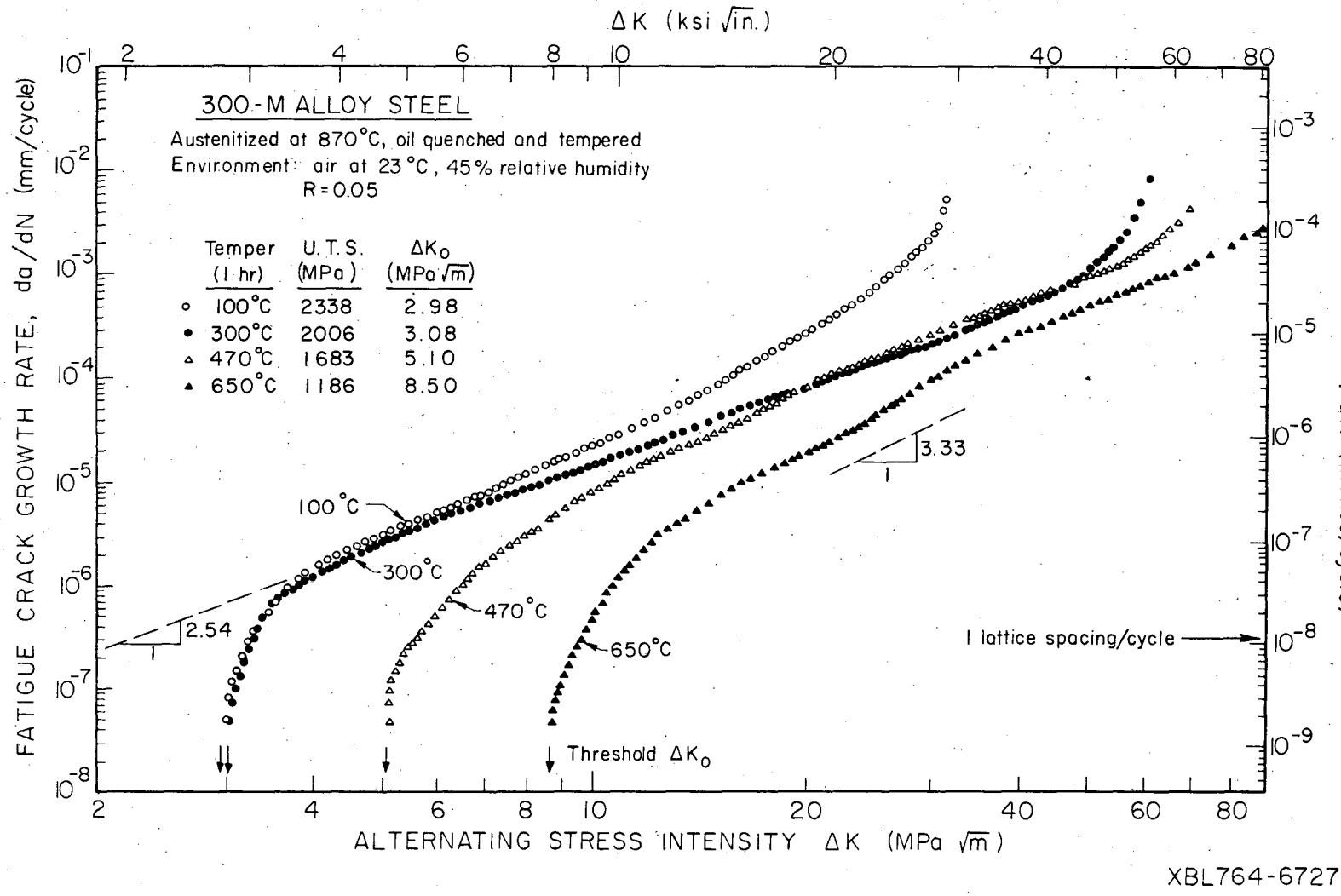

Fig. 4. Variation of fatigue crack growth rate (da/dN) with alternating stress intensity (ΔK) at R=0.05, for 300-M steel, quenched and tempered between 100°C and 650°C.

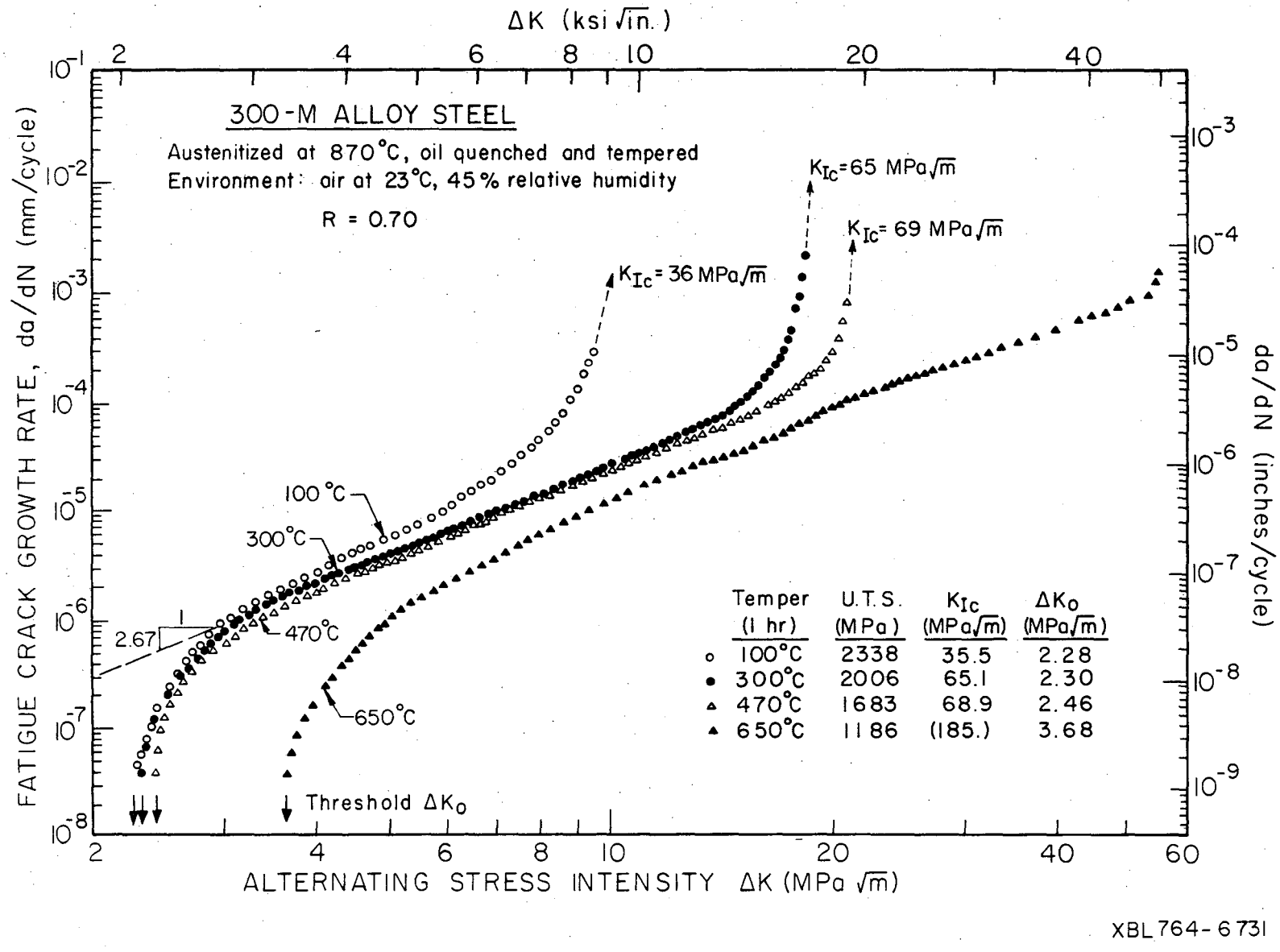

XBL 764-6731

Fig. 5. Variation of fatigue crack growth rate (da/dN) with alternating stress intensity (ΔK) at R=0.70, for 300-M steel, quenched and tempered between 100°C and 650°C.

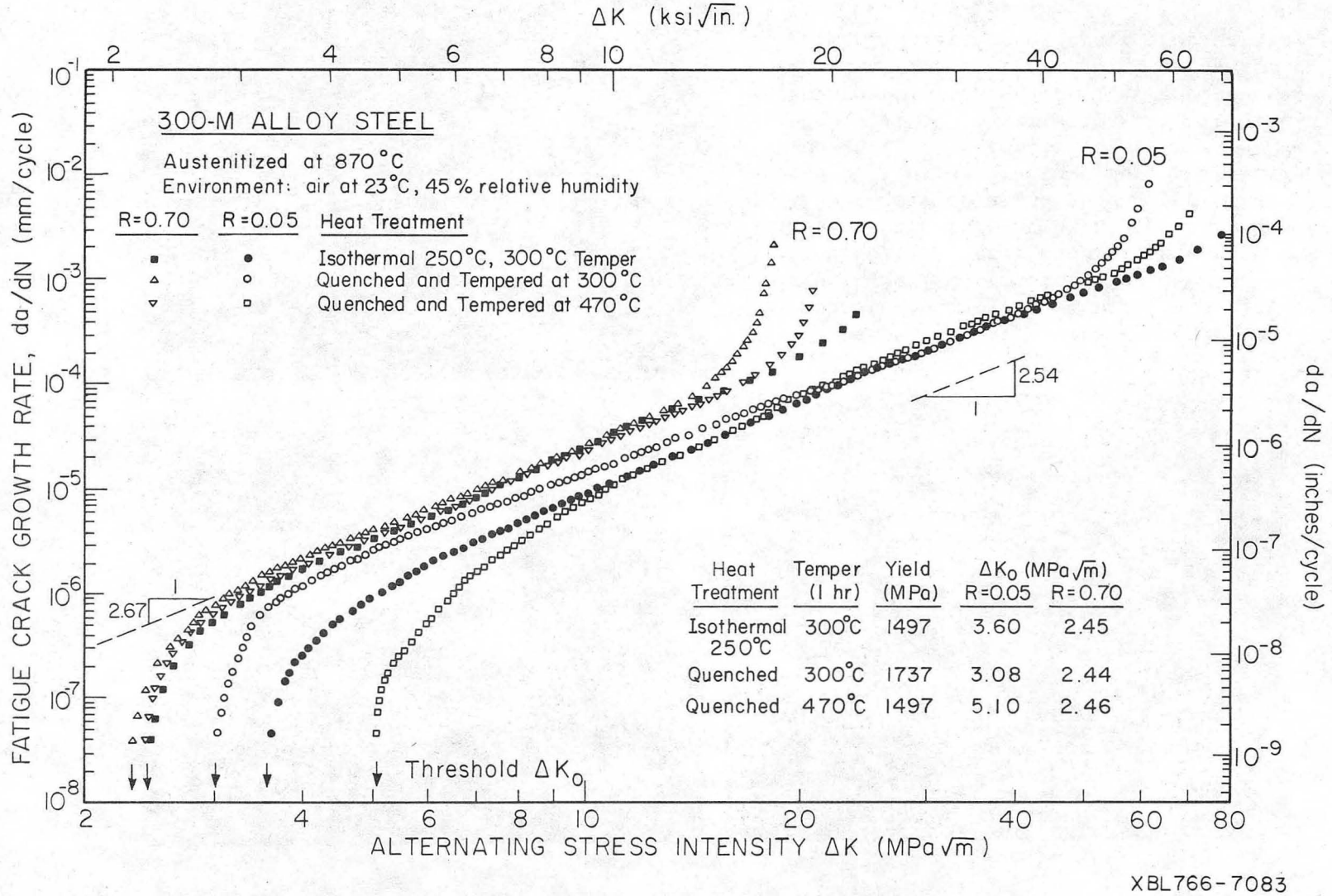

XBL766-7083

Fig. 6. Variation of fatigue crack growth rate (da/dN) with alternating stress intensity (ΔK) at R=0.05 and 0.70, for 300-M steel isothermally transformed at 250°C (ISO250). Results are compared with 300-M steel, quenched and tempered i) at the same temperature (T300) and ii) to the same monotonic yield strength (T470).

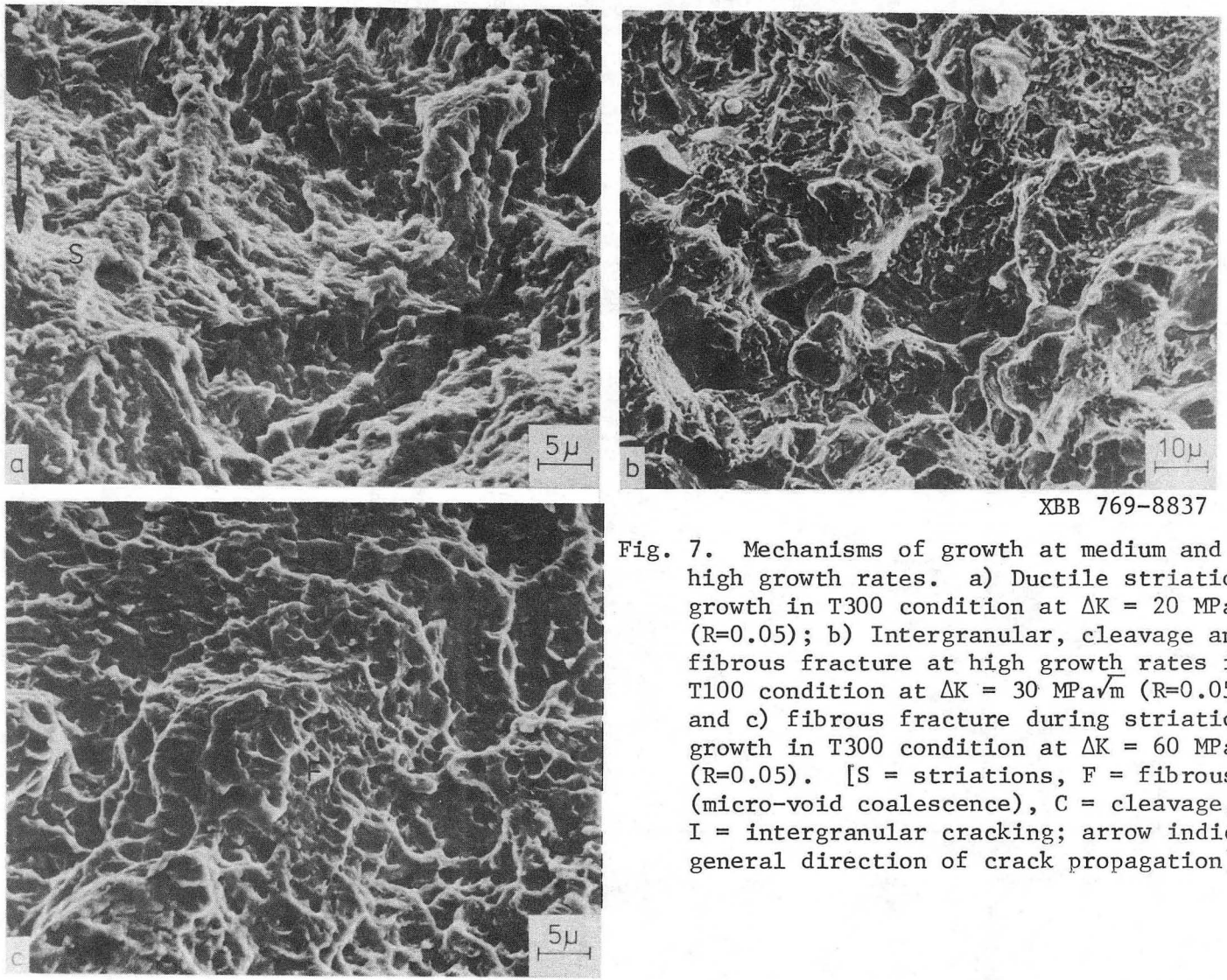

XBB 769-8837

Fig. 7. Mechanisms of growth at medium and high growth rates. a) Ductile striation growth in T300 condition at ΔK = 20 MPa$\sqrt{m}$ (R=0.05); b) Intergranular, cleavage and fibrous fracture at high growth rates in T100 condition at ΔK = 30 MPa$\sqrt{m}$ (R=0.05); and c) fibrous fracture during striation growth in T300 condition at ΔK = 60 MPa$\sqrt{m}$ (R=0.05). [S = striations, F = fibrous (micro-void coalescence), C = cleavage, I = intergranular cracking; arrow indicates general direction of crack propagation].

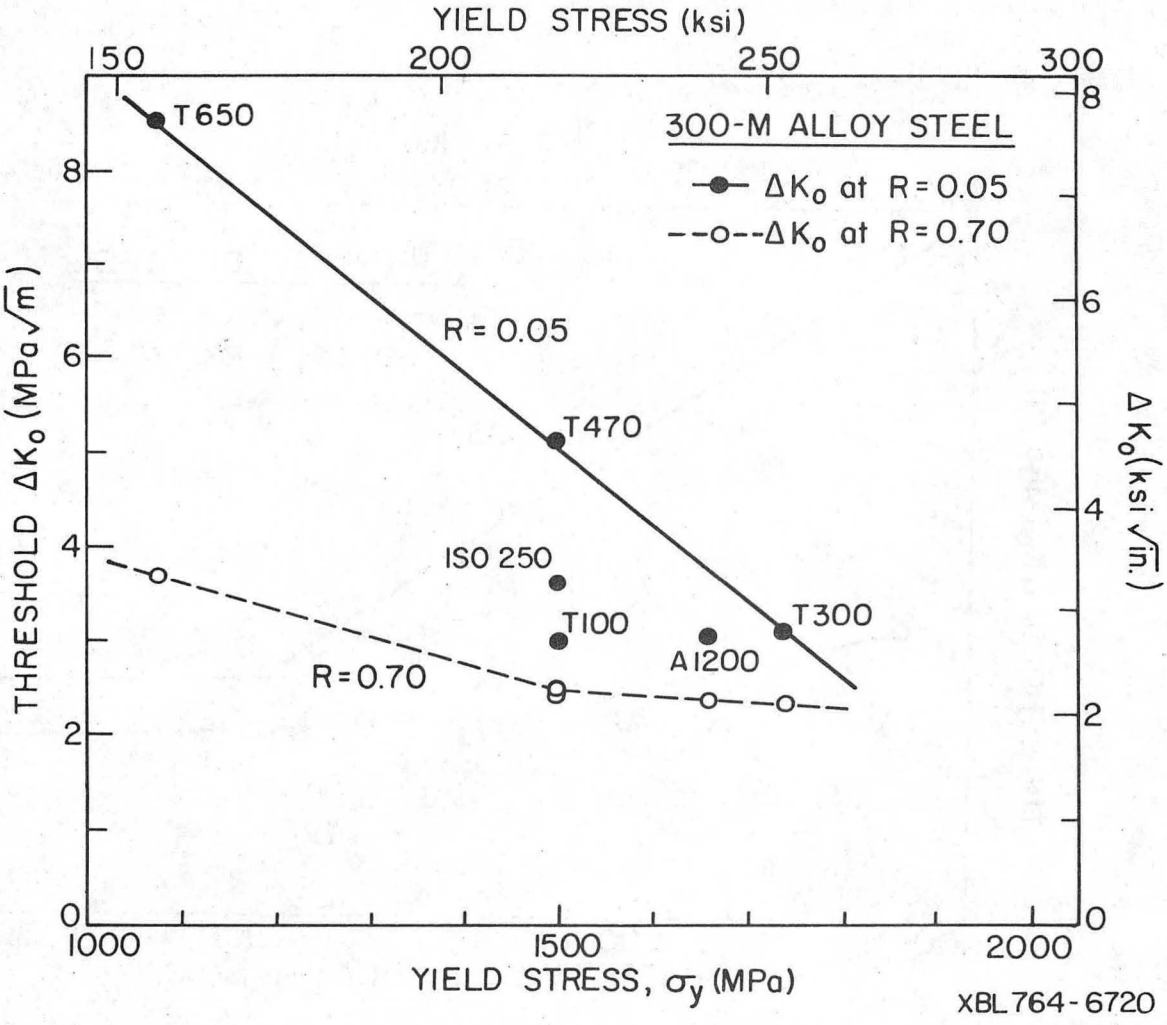

Fig. 8. Influence of monotonic yield strength (σ_y) on threshold for fatigue crack growth (ΔK_o) at R=0.05 and 0.70, in 300-M, tested in moist air.

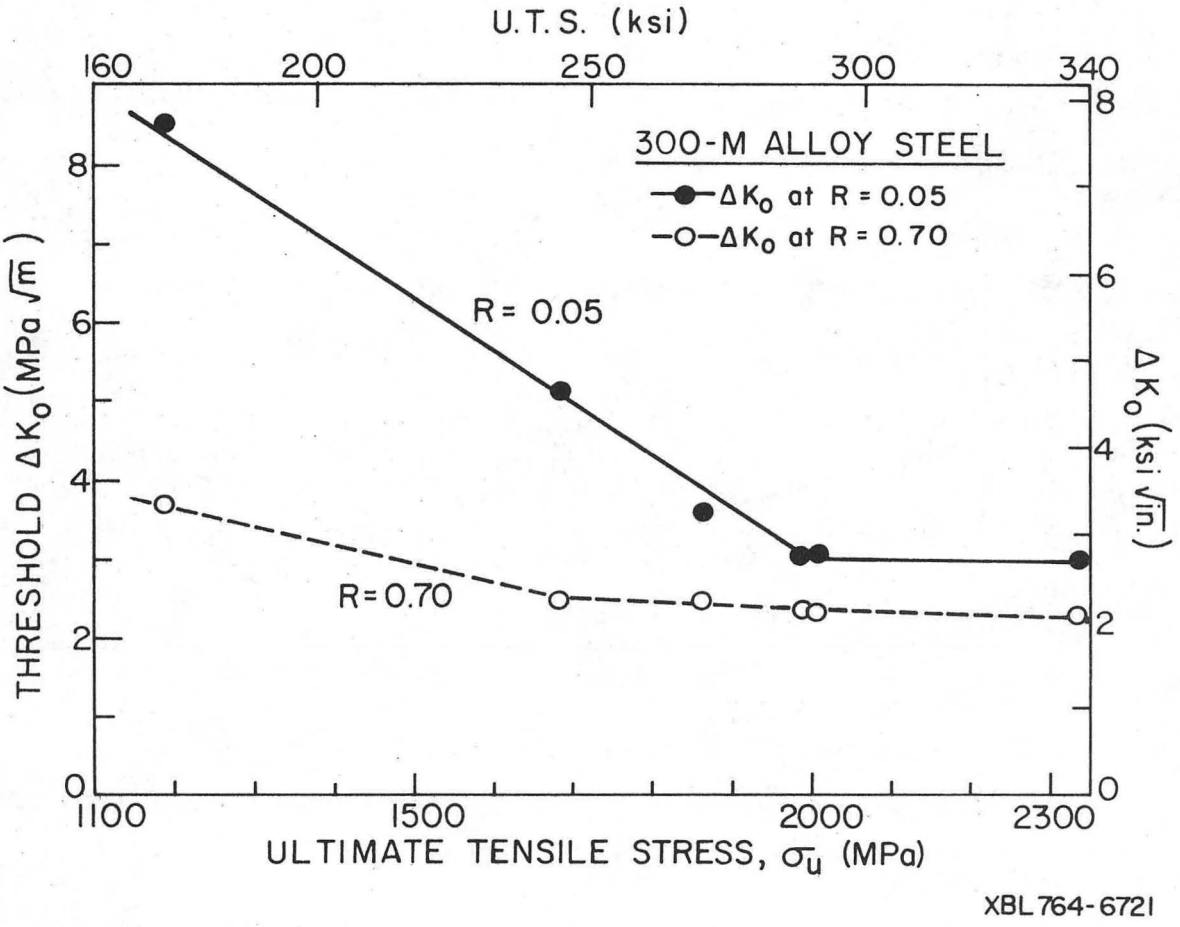

Fig. 9. Influence of ultimate tensile strength (U.T.S.) on threshold for fatigue crack growth (ΔK_o) at R=0.05 and 0.70, in 300-M, tested in moist air.

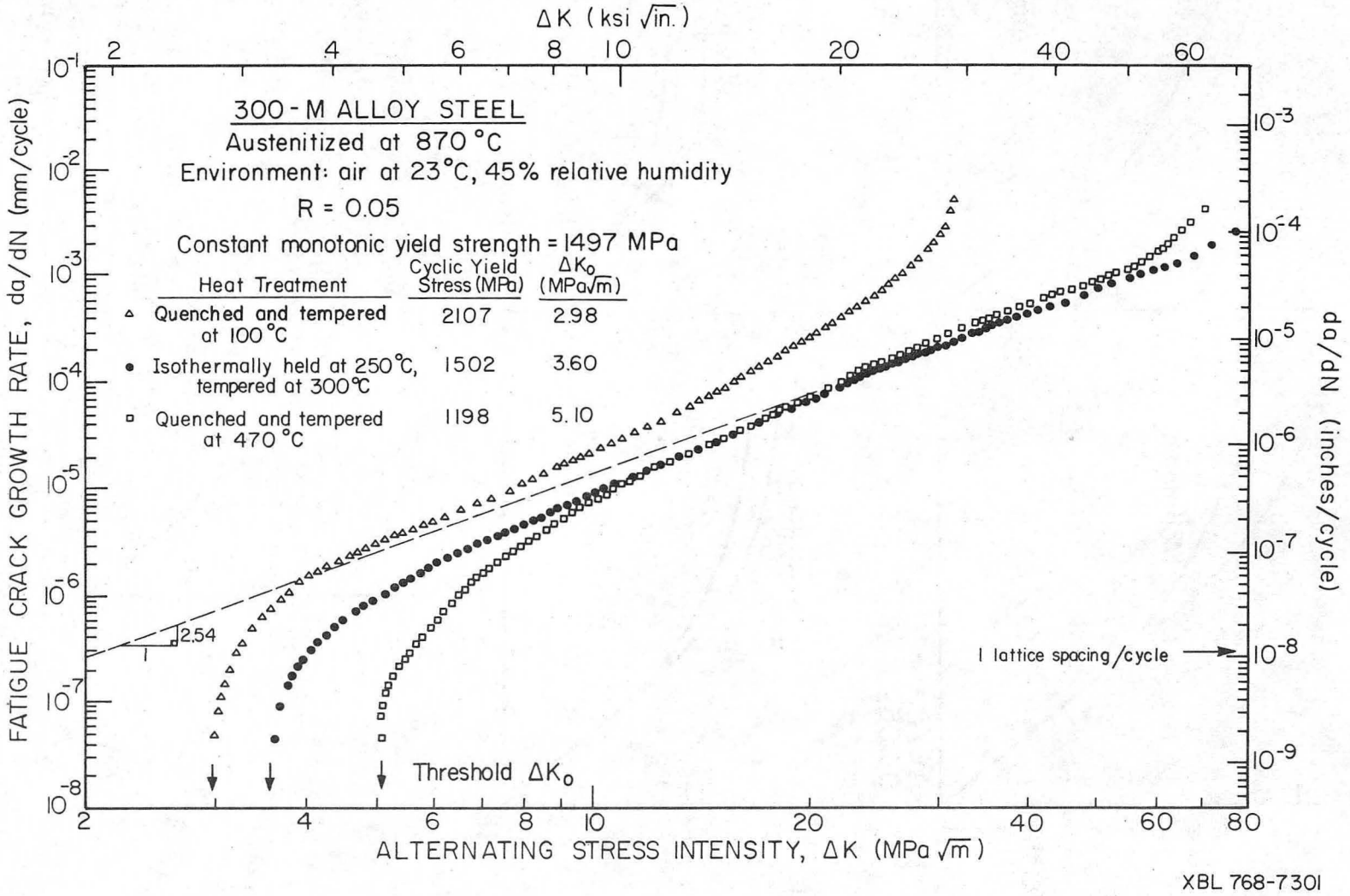

XBL 768-7301

Fig. 10. Comparison of fatigue crack growth behavior at R=0.05 of T100, T470 and ISO250 structures which show identical monotonic yield strength, but differing cyclic hardening/softening response.

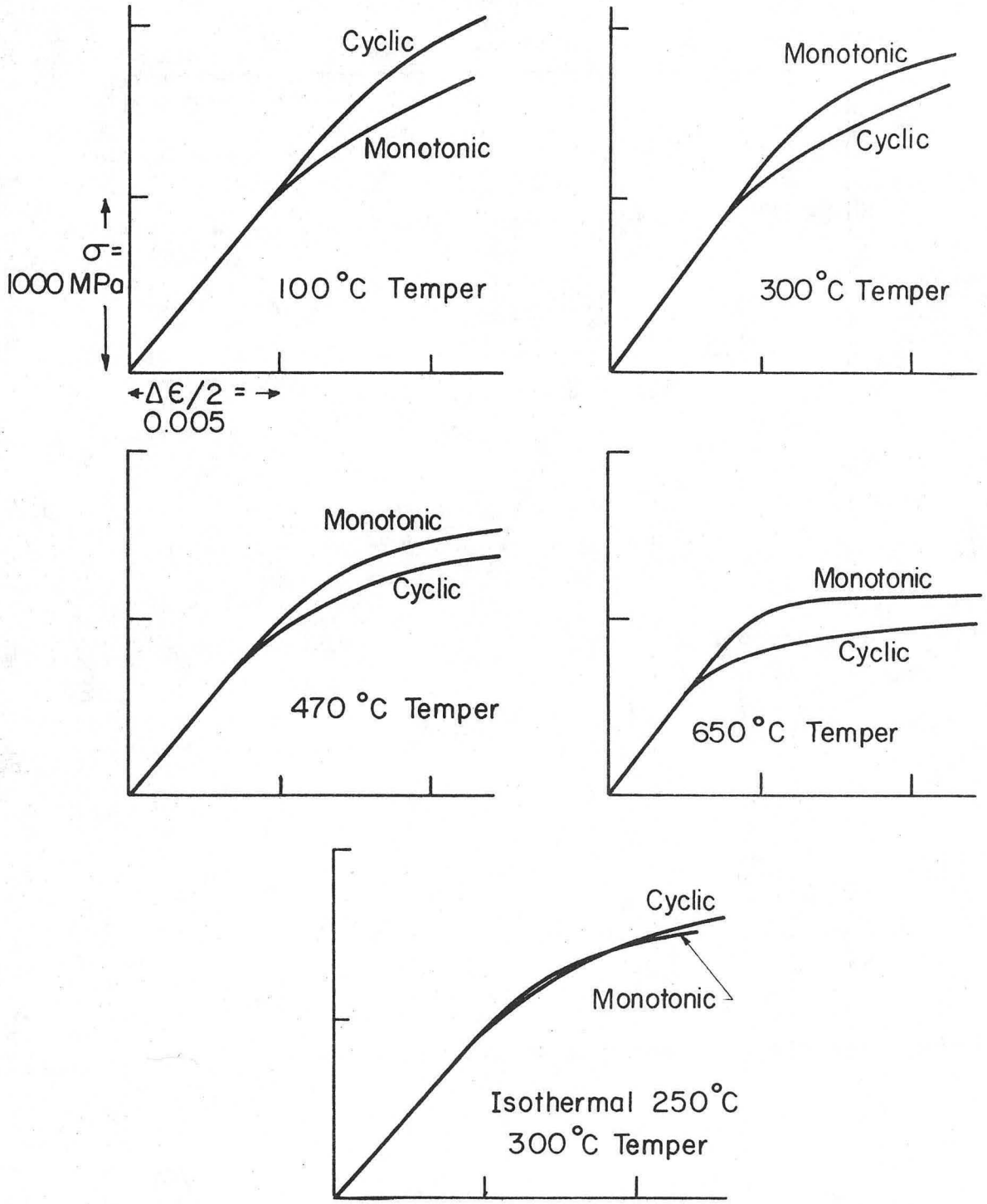

Fig. 11. Comparison of monotonic and cyclic stress-strain curves for 300-M steel, after quench and tempering and isothermal transformation heat-treatments.

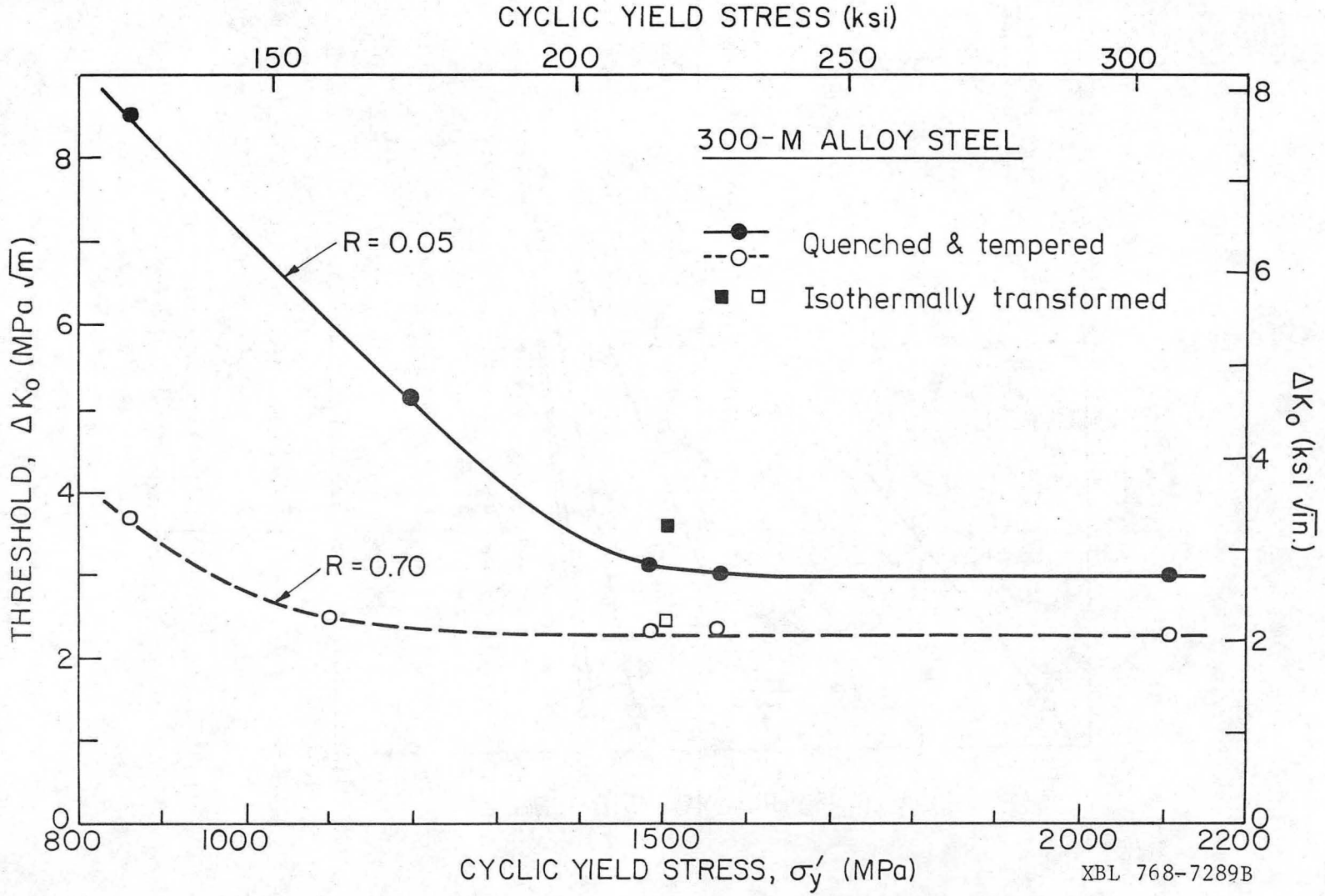

Fig. 12. Influence of cyclic yield strength ($\sigma_{y'}$), measured by 0.2% offset, on threshold for fatigue crack growth (ΔK_o) at R=0.05 and 0.70, in 300-M steel, tested in moist air.

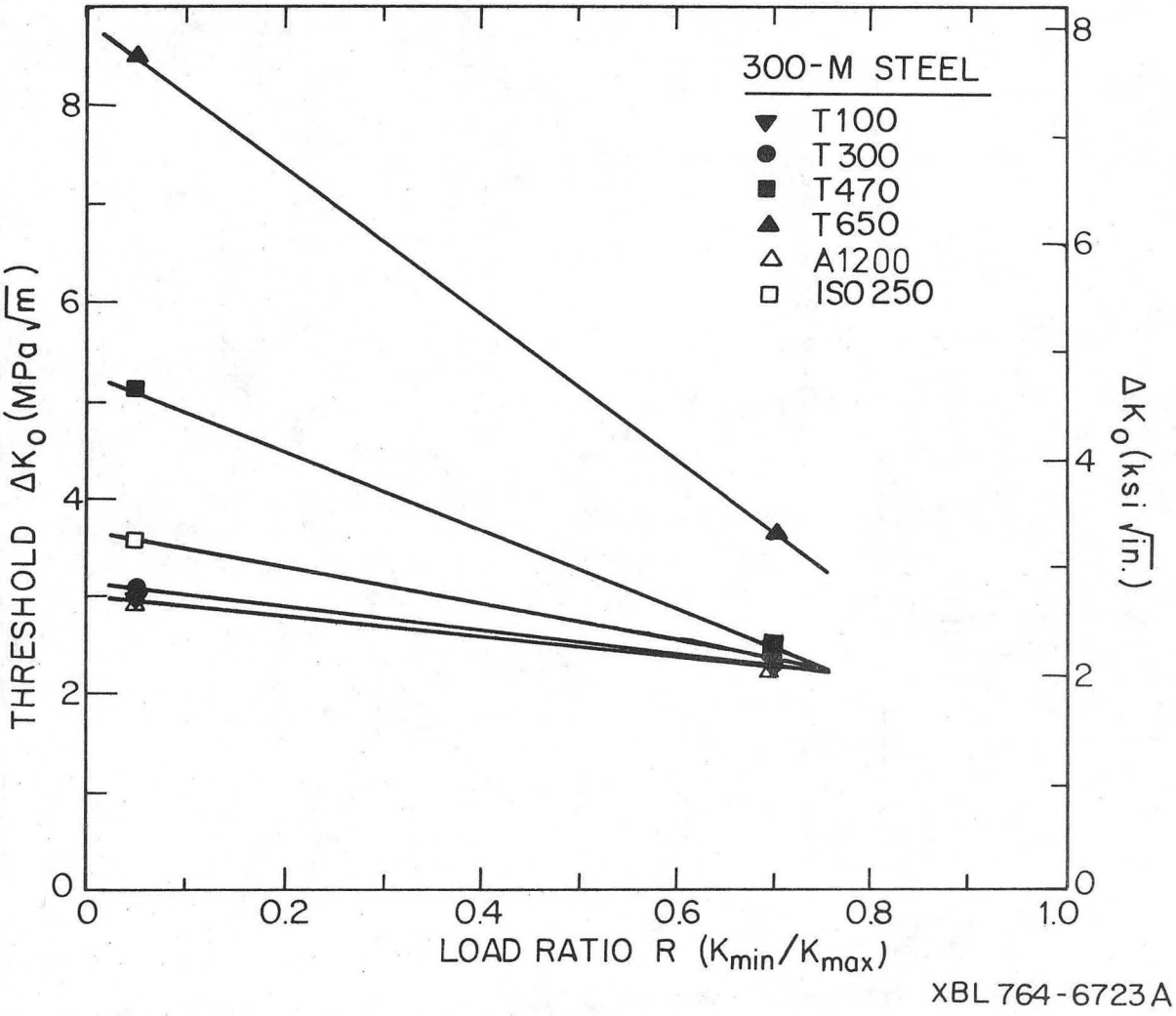

Fig. 13. Threshold for fatigue crack growth (ΔK_o) versus load ratio ($R=K_{min}/K_{max}$), at R=0.05 and 0.70, for 300-M steel.

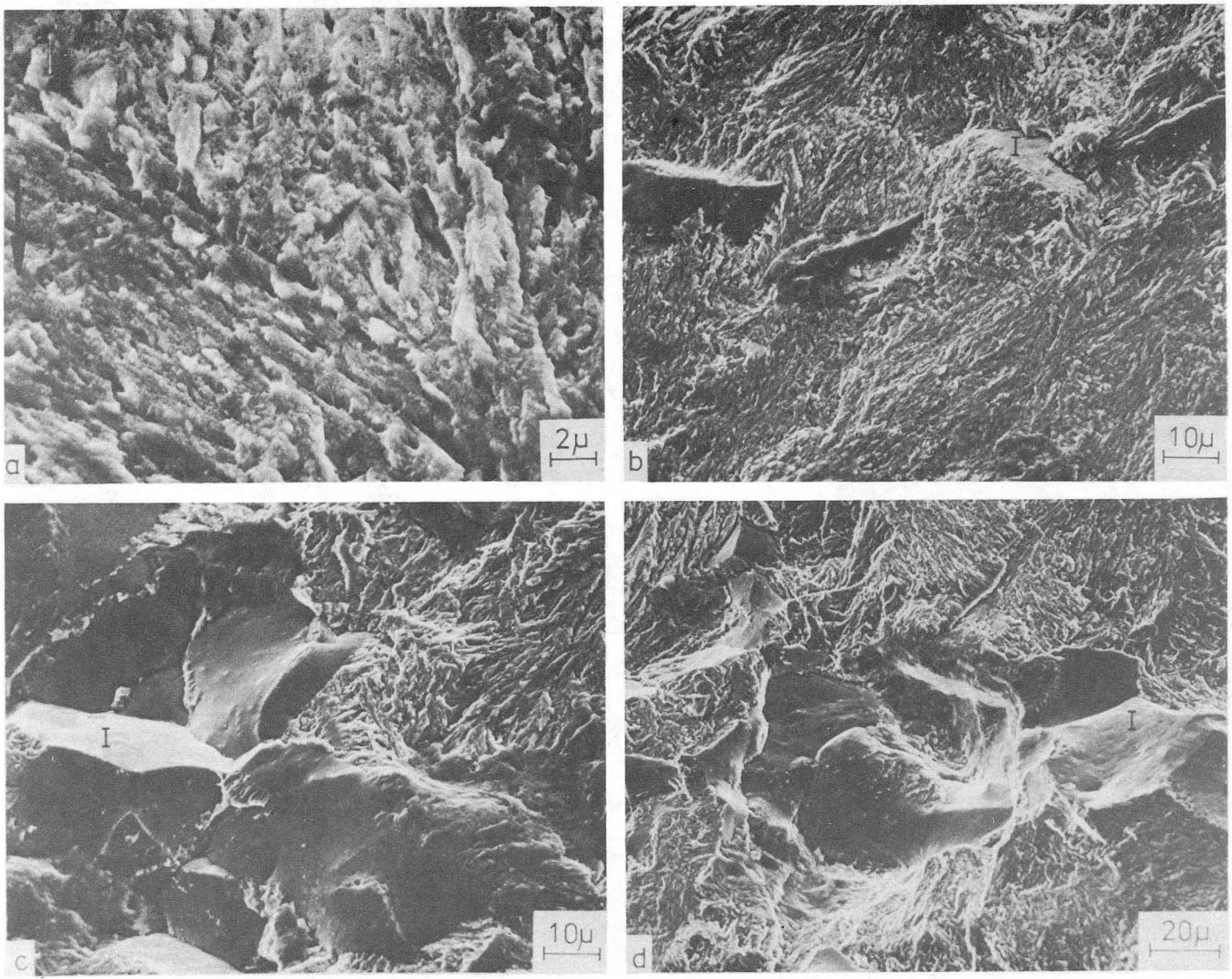

XBB 769-8836

Fig. 14. Mechanisms of growth at low growth rates, showing ductile transgranular mechanism with segments of intergranular fracture (I), in T470 condition at R=0.05. a) & b) At threshold, $\Delta K = 5.2$ MPa$\sqrt{m}$ ($\Delta K_o = 5.1$ MPa$\sqrt{m}$), c) $\Delta K = 7.6$ MPa$\sqrt{m}$, and d) $\Delta K = 11$ MPa$\sqrt{m}$. [Arrow indicates general direction of crack propagation].

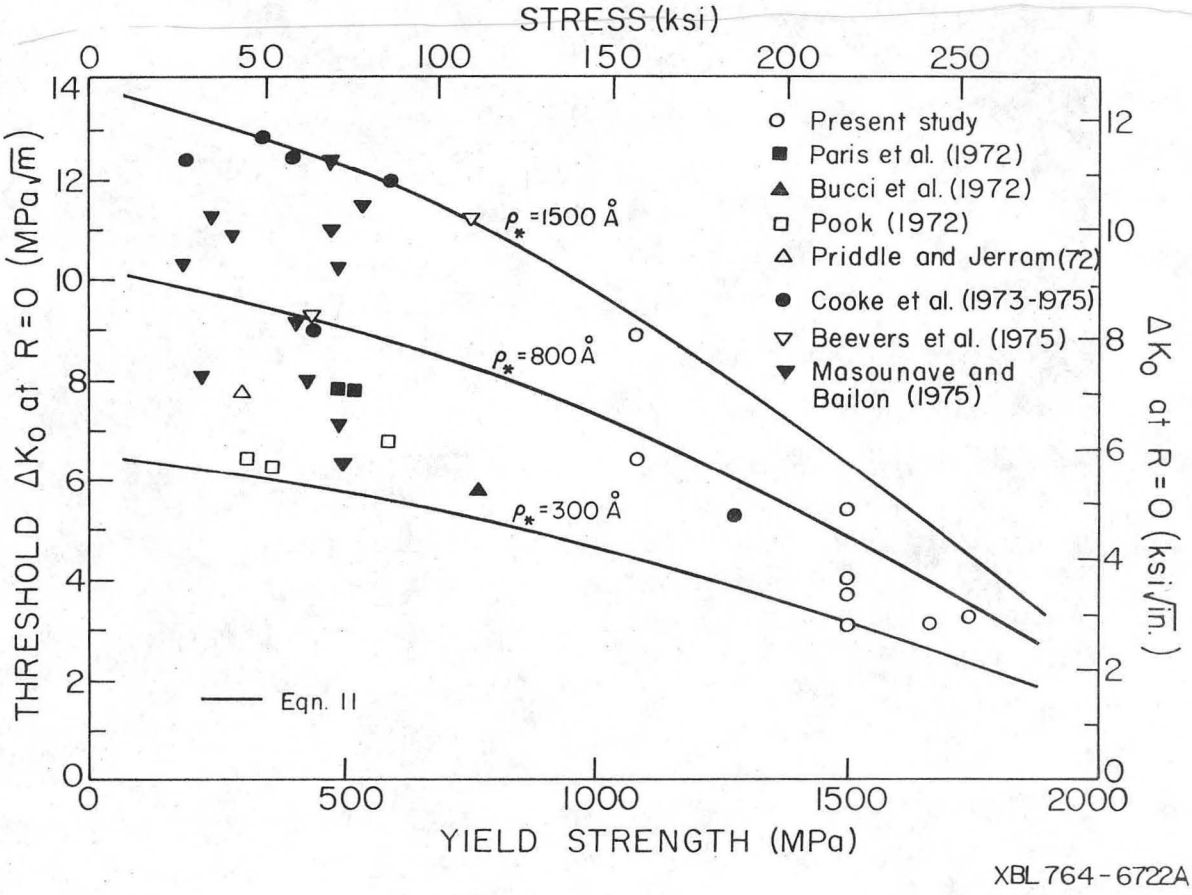

Fig. 15. Summary of results showing variation of threshold for fatigue crack growth (ΔK_o) at R=0 with yield strength for steels. Solid lines from threshold model (Eq. 11).

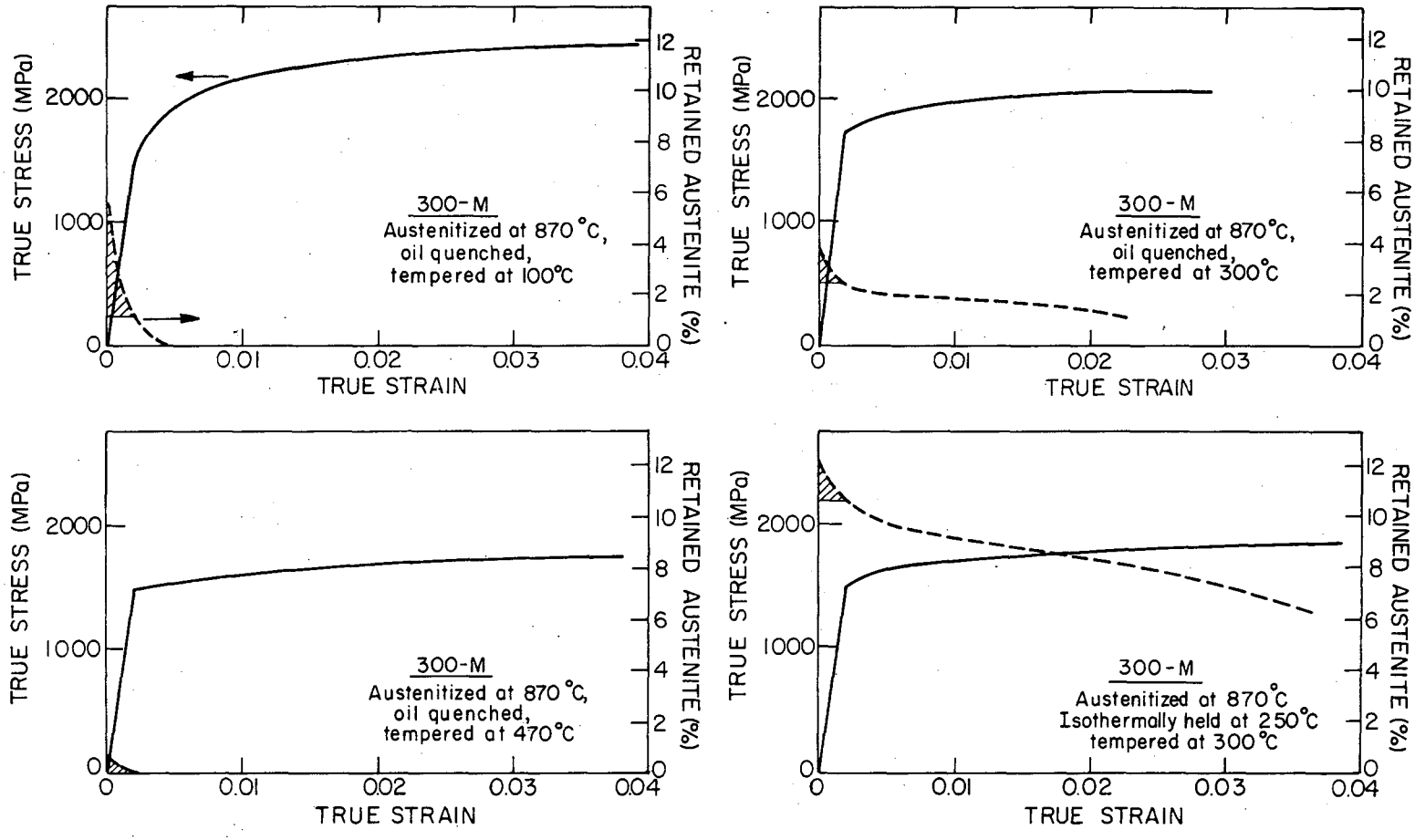

Fig. 16. Mechanical stability of retained austenite in quenched and tempered and isothermally transformed 300-M with respect to strain. True stress-true strain curves are plotted, superimposed with the amount of untransformed austenite. Shaded areas represent the amount of austenite transformed prior to yield (equivalent to stress-assisted transformation).

TECHNICAL INFORMATION DIVISION
LAWRENCE BERKELEY LABORATORY
UNIVERSITY OF CALIFORNIA
BERKELEY, CALIFORNIA 94720